IEEE ComSoc IEEE Communications Society
IEEE Open Journal of the Communications Society

Received 23 September 2024; revised 30 October 2024; accepted 28 November 2024. Date of publication 4 December 2024; date of current version 16 December 2024.

Digital Object Identifier 10.1109/OJCOMS.2024.3510882

Statistical Characterization of the Delay and Performance Analysis in 3-D Relay Networks

HADI HASHEMI[1], MARYAM OLYAEE[2], BEATRIZ SORET[2] (Senior Member, IEEE), M. CARMEN AGUAYO-TORRES[2] (Senior Member, IEEE), AND STEFANO BUZZI[3,4] (Senior Member, IEEE)

[1]Department of Electrical and Computer Engineering, University of Granada, 18071 Granada, Spain
[2]Telecommunication Research Institute (TELMA), Universidad de Málaga, 29017 Málaga, Spain
[3]Department of Electrical and Information Engineering, University of Cassino and Southern Lazio, 03043 Cassino, Italy
[4]Dipartimento di Elettronica, Informazione e Bioingegneria, Politecnico di Milano, 20133 Milan, Italy

CORRESPONDING AUTHOR: B. SORET (e-mail: bsoret@ic.uma.es)

This work was supported by the Spanish Ministerio de Ciencia, Innovación y Universidades (TATOOINE) under Grant PID2022-136269OB-I00. The work of Maryam Olyaee was supported in part by the Junta de Andalucía and the European Fund for Regional Development FEDER under Project P21-00420. The work of Stefano Buzzi was supported in part by the European Union under the Italian National Recovery and Resilience Plan (NRRP) of NextGenerationEU, with Reference to Partnership on "Telecommunications of the Future" (Program "RESTART," Structural Project NTN, Cascade Call INFINITE) under Grant PE00000001, and in part by the PRIN 2022 Project titled "INSPIRE: Integrated Terrestrial/Space Wireless Networks for Broadband Connectivity and IoT Services" (CUP: D53D23001150006) funded by the Italian MUR under Grant 2022BEXMXN_01.

ABSTRACT This article investigates a multi-tier 3D network that models a hybrid space-air-ground communication system and two main relay scenarios. In the first scenario, the aerial tier, consisting of entities such as Unmanned Aerial Vehicles (UAVs) or aircrafts, uses the space layer, represented by satellites, to connect to ground User Equipment (UE) devices or ground stations. In the second scenario, the space layer cooperates with satellites in a lower orbit or with aerial devices to communicate with ground-based devices. In both scenarios, it is assumed that the device acting as a relay is distributed throughout its tier according to a Poisson Point Process (PPP), and randomly selected from the coverage area that depends on the position of the source and destination devices. For both scenarios, the paper calculates the distribution function for the link distance, which permits to obtain the average delay of signal propagation. Further, in the paper the outage capacity and ergodic rate expressions for the amplify and forward (AF) and decode and forward (DF) relaying strategies under the shadowed-Rician fading channel model are derived. Also, the asymptotic behavior in the high-SNR regime is analyzed. These novel analytical expressions provide insights of the fundamental performance limits of integrated terrestrial and non-terrestrial wireless networks.

INDEX TERMS Multi-tier network, aerial layer, space layer, amplify and forward (AF) relay, decode and forward (DF) relay, distance distribution, stochastic geometry, satellite, propagation delay.

I. INTRODUCTION

TO FULFILL the promise of ubiquitous and seamless service, the sixth generation (6G) will bring a landscape of flying communication nodes at different altitudes, transmission powers, and capabilities [1]. Non-Terrestrial Networks (NTN), the term that encompasses the 3rd Generation Partnership Project (3GPP) standardization work, divides the sky into an aerial and a space segment [2]. The aerial layer consists of airplanes, Unmanned Aerial Vehicles (UAVs), High Altitude Platforms (HAPS), and other low-cost and high-mobility flying vehicles, which can take the role of User Equipment (UE) or Base Station (BS) depending on the application. The space segment, on the other hand, is populated with satellites in different orbits: Low-Earth Orbit (LEO), Medium-Earth Orbit (MEO), or Geostationary Orbit (GEO). In low orbits, LEO satellite constellations with hundreds or thousands of moderately-sized devices [3], [4] have received a lot of

attention in the last few years, and several commercial missions are providing service or are planned for the near future [5].

The initial standardization work concluded within the fifth generation (5G) scope, treats layers – or tiers – separately [6], [7]. The evolution from 5G to beyond-5G and 6G networks involves the native and complete support of a truly 3D architecture and the integration of the space and aerial layers with the existing terrestrial infrastructure, which represents itself an additional layer. In order to gain insight on the potentialities of such 3D three-layers architecture, a first step is to understand the performance limits of this network, under the assumption that the interconnected tiers are characterized by different transmission powers and coverage. This approach presents analogies with the 2D Heterogeneous Network (HetNet) paradigm first proposed more than one decade ago when designing the fourth generation of wireless networks [8].

Among all possible scenarios and network configurations, this paper addresses the situation where one of the layers is used as a relay to enhance connectivity. The relevance of this scenario is motivated by the fact that not all layers may have global and real-time coverage, and/or the capability to establish a connection to any other layer (e.g., airplanes over the ocean can be served by satellites but not from ground-based network elements). In contrast, interlayer cooperation can be realized in the form of relaying, to meet the 6G requirement of ubiquitous connectivity [9]. In our analysis, in order to capture the impact that the topology density and the large inter-node distances, which dominate the radio propagation losses, have on the performance of the considered radio links, we resort to the tool of stochastic geometry, which has been proven to be extremely powerful to model and analyze the spatial distribution and performance of terrestrial networks [10], [11], [12] and, more recently, dense satellite networks [13].

A. STATE-OF-THE-ART AND RELATED WORKS

In the context of 4G and 5G, Poisson processes and stochastic geometry have provided results for interference power, coverage probability, and latency in different scenarios; see an overview in [14]. In space, the model based on spatial statistics and stochastic geometry has recently been proven to be a suitable model for dynamic network topology analysis [13]. Specifically, the existing literature has modeled the LEO satellite locations as Poisson Point Process (PPP), Binomial Point Process (BPP) and non-homogeneous Poisson point process (NPPP) [15], [16], [17], [18], [19]. The authors in [15] consider satellites in uplink systems where devices are randomly distributed at arbitrary altitudes according to homogeneous BPP and attempt to eavesdrop on signals that a ground terminal transmits to a serving satellite. The authors in [16] modeled the LEO network as a NPPP with a variable density that depends on the size of the constellation, the altitude of the constellation and the inclination of the orbital planes. In [17] an analytical solution is presented for the downlink coverage probability and the average data rate of generic LEO networks, using stochastic geometry to abstract these networks into uniform BPP. The study [18] investigates the performance of an LEO satellite communication system, focusing on the probability of user coverage in a scenario where satellite gateways are deployed on the ground to act as relays and the LEO satellites are modeled as a BPP on a spherical surface. The study [19] examines the contact distance and nearest-neighbor distance statistics for BPPs on spherical surfaces, considering N concentric spheres with uniformly distributed points on their surfaces, such as LEO satellites. Homogeneous BPP is an excellent substitute for both the Fibonacci lattice-based point set and orbit model-based point process as a point process suitable for theoretical analysis. For a point process set with a lower altitude and a larger number of points, such as a point process based on a massive LEO satellite constellation, BPP has a better substitution effect, according to the results obtained in [20].

Stochastic geometry provides insights into the optimal design of satellite constellations and the complex interaction between satellites. Specifically, it enables the evaluation of coverage performance, including the determination of the outage capacity, the probability of coverage and outage, the capacity limits, interference, and characterizing the achievable data rates. In [21], it is assumed that the satellite is a relay in a network and wants to communicate between two devices on the ground. Satellites on the LEO surface are randomly distributed and no special constellation is considered for them. For this model, the coverage probability and the achievable data rate have been studied, and the statistical behavior of the communication angle has been analyzed. In [22], a cooperative satellite-aerial-terrestrial network is considered, where satellites or UAVs act as relays in fixed positions. Around the destination, there are some jammers whose distance models are treated as geometric problems, and the Probability Density Function (PDF) of the distances is calculated. For this model, the outage probabilities over the uplink and downlink are derived. There are several other articles with similar models for satellite-aerial-terrestrial that can be referred to [23], [24], [25]. In [26] throughput, energy efficiency and delay outages have been studied. In the performance calculations, the effect of distance was considered in the problem model, and based on the assumed model, a range for distance changes was obtained, and in the system performance analysis, a random value in this range was assumed and the results were obtained. Finally, [27] considers the multi-tier case of a satellite constellation with orbital planes at different altitudes, and studies the performance of the multi-hop routing on the space segment. Despite numerous related works having addressed important aspects of the problem, we notice that none of them has considered the spherical geometry of the relaying layer for the evaluation of the stochastic distribution of the distance, but rather assumed a fixed position. Therefore, our objective is to provide the

analysis of the general 3D multi-tier network with random positions of the relaying nodes, and its application to the performance evaluation of the system.

B. CONTRIBUTION

It should be noted that many existing works analyze separately the different layers, i.e., air and space orbits; however, the envisioned 6G multi-tier network relies on inter-layer connection and global coverage. More precisely, this paper focuses on the relaying of information between layers, a key functionality due to the large distances and heterogeneous technologies within the system. Taking the three-tiers case, i.e., ground, air, and space, we address two representative relaying scenarios, one where the space-layer acts as a relay (*Scenario I*) and another one where the air-layer is the relaying layer (*Scenario II*) (see Fig. 1). In particular, with regard to these two scenarios, the paper provides the following contributions:

1) A theoretical framework is introduced for analyzing an integrated ground-air-space system modeled as a multi-tier 3D relaying network and using Poisson processes and spatial statistics.
2) The closed form expressions of the PDF and cumulative distribution function (CDF) of the link distance is derived in the two scenarios, based on the location of the source and of the destination in the different possible states. This analysis requires using spatial statistics and geometry in spheres in order to find the coverage intersection conditions that ensures connectivity.
3) The average communication delay is calculated based on the derived distribution of the link distances.
4) The obtained distance probability distribution is exploited to analyze the system performance, specifically the calculation of the outage capacity and the ergodic rate metrics for two relaying strategies, amplify and forward (AF) and decode and forward (DF). The former is the simplest relaying solution and applicable when the SNR at the relay is not too low, whereas the latter is necessary for high reliability and weak signals arriving at the relay, at the cost of complexity and processing delays. The two metrics are obtained under the shadowed-Rician fading channel model. In addition, the asymptotic value of the metrics is also calculated for the case where the SNR in the first link is very high.
5) Finally, a thorough analysis is provided, discussing the impact of device position within tiers, of inter-device distance, and of the signal reception range on all relationships.

This paper is organized as follows. Section II introduces the system model. Subsequently, Sections III and IV examine the statistical behavior of the distances from source to relay and from relay to destination, respectively. Section V develops the formulation for the average propagation delay throughout the entire signal path. Section VI discusses how the results related to distances are applied. The simulation and numerical findings are presented in Section VII. Finally, concluding remarks are given in Section VIII.

TABLE 1. Variables definition.

Variable	Definition
r_e	Earth radius
r_D	Destination device radius
r_S	Source device radius
r_R	Relay device radius
β_D	Destination device angle to the equator
R	Radius of a given device on the upper tier
r	Radius of a given device on the lower tier
d	Distance between two devices on different tiers
θ	Angle between a link and horizon
θ_u	Minimum possible value of θ
d_{min}, d_{max}	Minimum and maximum value of d
ψ	Viewing angle for a device
$\psi_{S_{max}}$	Maximum viewing angle of the source
$\psi_{D_{max}}$	Maximum viewing angle of the destination
θ_D	Field of view of the destination
θ_S	Field of view of the source
d_1	Random distance between the source and a relay (Link 1)
d_2	Random distance between a relay and the destination (Link 2)
$d_{1_{min}}$, $d_{1_{max}}$	Minimum and maximum value of d_1
$d_{2_{min}}$, $d_{2_{max}}$	Minimum and maximum value of d_2
α_R	The colatitude angle of relay
β_R	The longitude angle of relay
$\beta_{R_{min}}$, $\beta_{R_{max}}$	Minimum and maximum value of β_R
L	Total length of the links
τ	Total delay
c	Speed of light
h_1	Fading channel of Link 1
h_2	Fading channel of Link 2
n_r, n_d	Gaussian noise at a relay and the destination
σ_r^2, σ_d^2	Noise variance at a relay and the destination
P, $\hat{P}$	Transmitted power at the source and a relay
s, $\hat{s}$	Signal at the source and a relay
C_{th}	Capacity threshold
Ω	Average power of the LOS
m	Nakagami-m fading parameter

C. NOTATION

Table 1 provides a summary of the key variables and parameters used throughout this paper, together with a brief description.

II. SYSTEM MODEL

Suppose that we have a multi-tier NTN where the signal is transmitted through a relay from the source to the destination. The ground surface can be recognized as the lowest tier of the network and is referred to as tier-ground. Without losing the

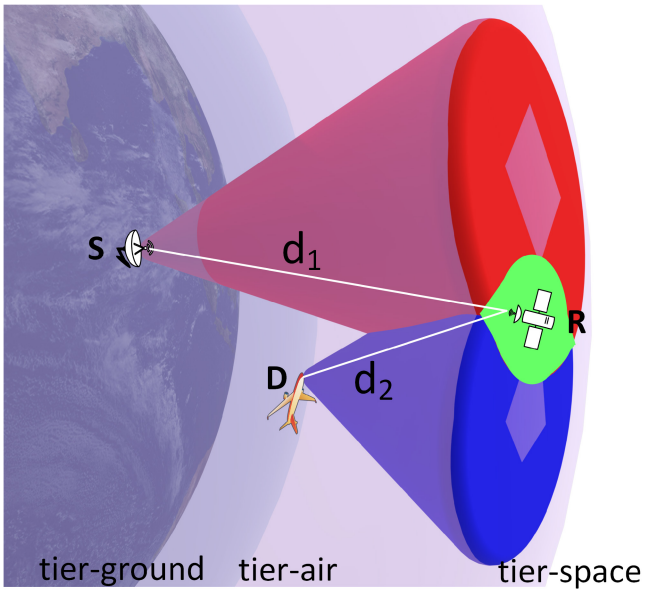

(a) System Model in Scenario I: a geometric representation of the source in the ground tier, relay in the space tier, and destination in the air tier.

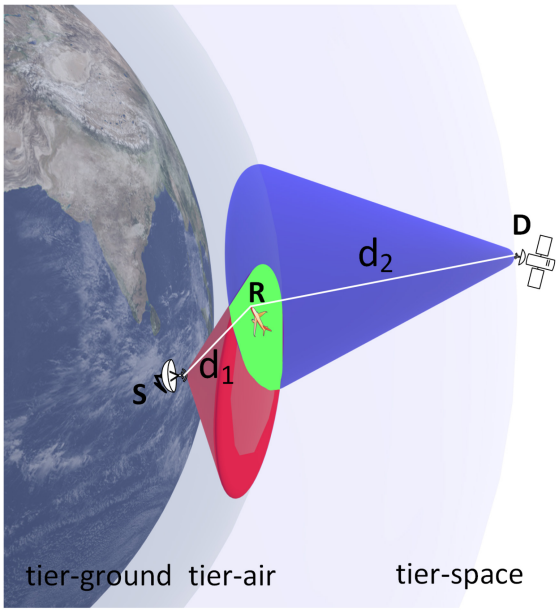

(b) System Model in Scenario II: a geometric representation of the source in the ground tier, relay in the air tier, and destination in the space tier.

FIGURE 1. The angle of view of the source is shown in the red cone and the angle of view of the destination is shown in the blue cone. In both scenarios, d_1 and d_2 represent Source-to-relay (Link 1) and relay-to-destination distance (Link 2), respectively.

generality of the problem, it is assumed that the source of the signal is in tier-ground with a fixed and specific location. The middle layer of this network is the tier-air, which can include the flying surface of an airplane or UAV, and the top and final tier is tier-space, which can be satellites at different orbital heights. Two different scenarios are considered to analyze the network. In Scenario I, we consider the transmission of a signal between tier-ground and an airborne vehicle in tier-air, and a relay is placed in tier-space to connect the source to the destination (See Fig. 1(a)). In Scenario II, the signal destination is considered to be in tier-space and a relay is considered to be in tier-air (See Fig. 1(b)). In both scenarios, the relay is assumed to be in a random location for a given source and destination location.

Due to obstacles such as buildings, towers, trees, and mountains, we assume that there is no direct link between the source and the destination. Directional signal transmission is considered to be the most efficient use of signal power on the network. Therefore, by considering the viewing angle for each device, it can only communicate with a relay device at an angle greater than θ to the horizon. In both scenarios, the random position of the relay is modeled as a BPP. As shown in Fig. 1, which presents the model for Scenarios I and II, respectively, a device on the tier-ground can communicate directly with a relay device inside the red cone, and the destination can communicate with a relay device inside the blue cone. Thus, the intersection of these two cones is on the tier where the relay is located and is shown in green.

For analysis in Cartesian coordinates, the origin is considered to be the center of the Earth, and the source device is located at radius r_e and angle zero to the equator. We have a plane containing the locations of the three devices at the ground, relay, and destination, which is a unique plane for given points. Therefore, the source coordinate can be written as follows,

$$POS_S = \begin{bmatrix} r_e \\ 0 \\ 0 \end{bmatrix}, \tag{1}$$

and the destination device, flying in a sphere with radius r_D and angle β_D to the equator, is located at

$$POS_D = \begin{bmatrix} r_D \cos(\beta_D) \\ r_D \sin(\beta_D) \\ 0 \end{bmatrix}. \tag{2}$$

Without considering any particular topology, assume that the relay is located on the sphere with radius r_R. This relay surface is in tier-space for scenario I and in tier-air for scenario II. According to the possible angular range for a device to transmit and receive a signal, the relay should be placed in an overlapping cap of this sphere to have a direct connection with both the source and the destination devices. The source-to-relay and relay-to-destination distances are random variables that depend on each other. We study their statistical behavior and then use them to evaluate network performance. Although not explicitly analyzed, a straightforward third scenario is the

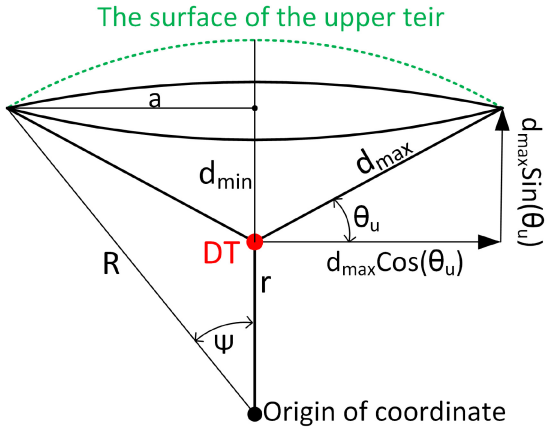

FIGURE 2. Two-dimensional representation of the field of view of a device in a lower tier and separation of the cap on the spherical surface in the upper tier.

one in which the source and destination are in tier-ground, corresponding to a conventional 2-tier relay.

In the following section, we will analyze the statistical behavior of distances. However, before proceeding, we require the following definition.

Definition 1: Assuming two devices are located in two different tiers with radii of r and R, where $r < R$. The parameter d is defined as the distance between point DT (device on tier) and a random point on the surface of the cap in Fig. 2, which has angle θ with the horizon and θ_u is the minimum value of θ. Using the mathematical operations from the schema depicted in Fig. 2, the smallest distance between these devices can be calculated

$$d_{min} = R - r \tag{3}$$

and the maximum distance is

$$d_{max} = \sqrt{R^2 - r^2\cos(\theta_u)} - r\sin(\theta_u). \tag{4}$$

For $d_{min} \le d \le d_{max}$, we have

$$\sin(\theta) = \frac{R^2 - d^2 - r^2}{2rd},$$
$$\cos(\theta) = \sqrt{1 - \frac{\left(R^2 - d^2 - r^2\right)^2}{4r^2d^2}}.$$

Therefore, the angle ψ which is the view angle from the origin, shown in Fig. 2, is calculated as

$$\psi = \sin^{-1}\left(\frac{d_{max}}{R}\cos(\theta_u)\right)$$
$$= \sin^{-1}\left(\frac{\sqrt{4r^2d_{max}^2 - \left(R^2 - d_{max}^2 - r^2\right)^2}}{2Rr}\right). \tag{5}$$

III. STATISTICAL BEHAVIOR OF THE DISTANCE BETWEEN THE SOURCE AND A RELAY (LINK 1)

In this section, we will study the PDF of the distance between the source and a relay in the network. To obtain this result, we must first determine the CDF of the distance. Regardless of the location of the relay in both scenarios, we refer to the link between the source and the relay as Link 1, and the link between the relay and the destination as Link 2.

Based on Definition 1, we can determine the maximum distance using eq. (4). Subsequently, the viewing angle range for each device will be calculated using eq. (5). In both scenarios, the maximum viewing angles for the source and destination are referred to as $\psi_{S_{max}}$ and $\psi_{D_{max}}$, respectively. The source device is in a lower tier in both scenarios, so $\psi_{S_{max}}$ is calculated using eq. (5) by applying $\theta_u = \theta_S$ and $d_{max} = d_{1_{max}}$. In Scenario I, the destination position is located on the tier-air (lower tier), and $\psi_{D_{max}}$ is also calculated applying Eq. (5), by $\theta_u = \theta_D$ and $d_{max} = d_{2_{max}}$.

However, in scenario II, the destination position is located on the tier-space (upper tier), and $\psi_{D_{max}}$ is obtained as follows

$$\psi_{D_{max}} = \tan^{-1}\left(\frac{r_D\tan(\theta_D) - \sqrt{\frac{r_R^2}{\cos^2(\theta_D)} - r_D^2}}{r_D + \tan(\theta_D)\sqrt{\frac{r_R^2}{\cos^2(\theta_D)} - r_D^2}}\right). \tag{6}$$

Based on the viewing angle range of the source and destination, there should be a common region (green area in Fig. 1) to be able to find a relay. The above parameters help us to figure out whether the common areas exist or not. Next, we categorize and analyze all potential situations based on four distinct states.

A. STATE A: $\beta_D > \psi_{S_{MAX}} + \psi_{D_{MAX}}$

In this case, the position of the source and destination and their range of view in the relay tier do not overlap. Therefore, it is not feasible to locate a device that can act as a relay between them, and the definition of the distance PDF will also be meaningless in this situation. This situation can occur in the network for two reasons: Firstly, the destination is situated at a considerable distance from the origin and β_D is of significant magnitude, resulting in the two cones having no overlap. Secondly, the devices' viewing angle is so narrow that their field of view is limited.

B. STATE B: $\beta_D < \psi_{D_{MAX}} - \psi_{S_{MAX}}$

In this situation, the field of view of the source is completely inside the field of view of the destination. This means that the entire area of a cap enables the connection to the relay and, as a result, we have to do all calculations based on the area of the entire cap. Fig. 3 shows a two-dimensional view of the problem. The total possible area of the cap is shown in green. Therefore, this is the common area between the fields of view of the two devices.

The random variable parameter d_1 as a source-to-relay distance, valued between $d_{1_{min}}$ and $d_{1_{max}}$. So, when the

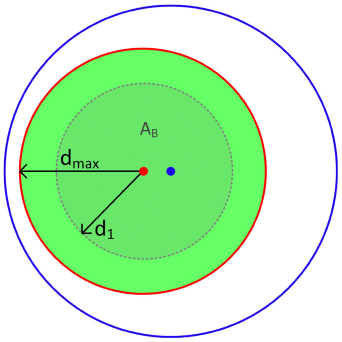

FIGURE 3. Two-dimensional map of the region covered by the source and destination and their common area in state $\mathcal{B}$. The red dot represents the position of the source and the red circle marks where the device's field of view intersects with the surface of the relay tier sphere. Similarly, the blue dot and circle indicate the destination.

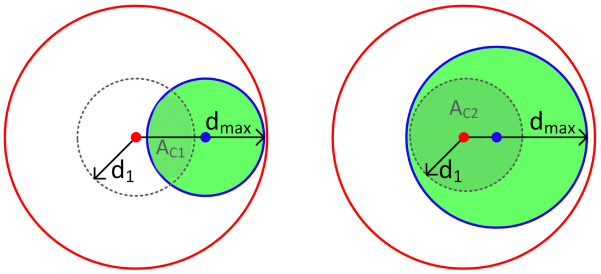

(a) State $\mathcal{C}1$ (b) State $\mathcal{C}2$

FIGURE 4. Two-dimensional map of the region covered by source and destination and their common area in state $\mathcal{C}$. The red dot represents the position of the source and the red circle marks where the device's field of view intersects with the surface of the relay tier sphere. Similarly, the blue dot and circle indicate the destination.

distance between the source and the relay is equal to $d_{1_{max}}$, the common area is given by

$$\begin{aligned}\Phi_{\mathcal{B}} &= 2\pi r_R\left(r_R - r_S - d_{1_{max}}\sin(\theta_S)\right)\\ &= 2\pi r_R\left(d_{1_{min}} - \frac{r_R^2 - d_{1_{max}}^2 - r_S^2}{2r_S}\right)\\ &= \frac{\pi r_R}{r_S}\left(d_{1_{max}}^2 - d_{1_{min}}^2\right).\end{aligned} \tag{7}$$

Similar to eq. (7), if we consider the value of the distance $d_{1_{min}} \le d_1 \le d_{1_{max}}$, the area is obtained as

$$A_{\mathcal{B}}(d_1) = \frac{\pi r_R}{r_S}\left(d_1^2 - d_{1_{min}}^2\right).$$

As a result, the CDF is obtained as

$$F_{D1}(x) = \frac{A_{\mathcal{B}}(x)}{\Phi_{\mathcal{B}}} = \frac{x^2 - d_{1_{min}}^2}{d_{1_{max}}^2 - d_{1_{min}}^2}, \tag{8}$$

and by taking its derivative, the PDF calculated as

$$f_{D1}(x) = \frac{2x}{d_{1_{max}}^2 - d_{1_{min}}^2}. \tag{9}$$

C. STATE $\mathcal{C}$: $\beta_D < \psi_{S_{MAX}} - \psi_{D_{MAX}}$

In this situation, the field of view of the destination is completely inside the field of view of the source. However, two modes for the statistical behavior of the distance can be imagined. One is when the destination field of views is not perpendicular to the source and the other is when the range has passed over the source. These two situations will be addressed separately below, and the distinction can be seen in Fig. 4.

1) STATE $\mathcal{C}1$ - WHEN THERE IS NO VERTICAL COVER ON THE SOURCE

In this situation, the possible distance between the source and destination can take a different range. Fig. 4(a) shows an example of this mode. The range of changes of d_1 is obtained in such a way that the minimum distance occurs when ψ is equal to $\beta_D - \psi_{D_{max}}$ and the maximum distance occurs when it is equal to $\beta_D + \psi_{D_{max}}$. Therefore,

$$\begin{aligned}d_{1_{min}} &= \sqrt{r_R^2 + r_S^2 - 2r_R r_S\cos\left(\beta_D - \psi_{D_{max}}\right)}\\ &\triangleq \chi\left(-\psi_{D_{max}}\right)\end{aligned} \tag{10}$$

and

$$d_{1_{max}} = \chi\left(\psi_{D_{max}}\right). \tag{11}$$

Now, similar to the steps taken for the previous state, the surface is obtained as

$$\Phi_{\mathcal{C}1} = \frac{\pi r_R}{r_D}\left(d_{2_{max}}^2 - d_{2_{min}}^2\right), \tag{12}$$

and the area of the desired section based on Fig. 4(a) is calculated as

$$\begin{aligned}A_{\mathcal{C}1}(d_1) = \Lambda\Big(\ & r_R, d_{2_{max}}\cos(\theta_D),\\ & \sqrt{d_1^2 - \frac{(r_D^2 - r_S^2 - d_1^2)^2}{4r_S^2}}, \beta_D\Big).\end{aligned} \tag{13}$$

$\Lambda(.,.,.,.)$ is the intersection area of two caps on the surface of a sphere as [28]

$$\begin{aligned}\Lambda(r_s, a_1, a_2, a_3) \triangleq\ & 2r_s^2\Big(\pi - \cos^{-1}\Big(\csc(t)\csc(u)\cos(a_3)\\ & - \cot(t)\cot(u)\Big) - \cos^{-1}\Big(\csc(t)\cos(u)\csc(a_3) - \cot(t)\\ & \cot(a_3)\Big)\cos(t) - \cos^{-1}\Big(\cos(t)\csc(u)\csc(a_3) - \cot(u)\\ & \cot(a_3)\Big)\cos(u)\Big),\end{aligned} \tag{14}$$

where

$$t = \sin^{-1}\left(\frac{a_1}{r_s}\right), u = \sin^{-1}\left(\frac{a_2}{r_s}\right),$$

r_s is the radius of the sphere, a_1 and a_2 are the radii of the caps, and a_3 is the angle between the centers of the two caps. Therefore, the CDF and PDF of d_1 in state $\mathcal{C}1$ are respectively achieve as

$$F_{D_1}(x) = \frac{A_{\mathcal{C}1}(x)}{\Phi_{\mathcal{C}1}} \tag{15}$$

and

$$f_{D_1}(x) = \frac{\partial F_{D_1}(x)}{\partial x} = \frac{\mathcal{P}(x)}{\Phi_{\mathcal{C}1}} \tag{16}$$

where $\mathcal{P}(.)$ is defined as follows,

$$\begin{aligned}\mathcal{P}(d) &= \frac{\partial}{\partial d}\Lambda\left(r_R, d_{2_{max}}\cos(\theta_D), \sqrt{d^2 - \frac{(r_R^2 - r_S^2 - d^2)^2}{4r_S^2}}, \beta_D\right) \\ &= \Pi_1(d) + \Pi_2(d) + \frac{\Pi_3(d)}{\Pi_4(d)} - \Pi_5(d),\end{aligned} \tag{22}$$

where the functions are obtained for those Π_i, $i \in \{1, 2, 3, 4, 5\}$ and written at the top of the next page, and in those

$$g_1(d) = 2d - d\frac{d^2 + r_S^2 - r_R^2}{r_S^2}$$

and

$$g_2(d) = d^2 - \frac{\left(d^2 + r_S^2 - r_R^2\right)^2}{4r_S^2}.$$

2) STATE $\mathcal{C}2$ - WHEN THERE IS A VERTICAL COVER ON THE SOURCE

As we can see in Fig. 4(b), the total area of the acceptable region is similar to the case of $\mathcal{C}1$. But in the calculation of the covered area up to the distance d_1, two modes are possible. First, when $d_{1_{min}} \leq d_1 \leq \chi(-\psi_{D_{max}})$, we have a complete cap corresponding to the distance d_1, so its area is obtained as

$$A_{\mathcal{C}2-1}(d_1) = \frac{\pi r_R}{r_S}\left(d_1^2 - d_{1_{min}}^2\right). \tag{23}$$

In the second case, as the value of d_1 increases, we have the intersection of two caps, which is similar to the state $\mathcal{C}1$, so,

$$\begin{aligned}A_{\mathcal{C}2-2}(d_1) = \Lambda(\ & r_R, d_{2_{max}}\cos(\theta_D), \\ & \sqrt{d_1^2 - \frac{(r_R^2 - r_S^2 - d_1^2)^2}{4r_S^2}}, \beta_D),\end{aligned} \tag{24}$$

where $\Lambda(.,.,.,.)$ is defined in (14). According to the above equations, the CDF and PDF of d_1 in state $\mathcal{C}$ are obtained respectively as

$$F_{D_1}(x) = \begin{cases} \frac{A_{\mathcal{C}2-1}(x)}{\Phi_{\mathcal{C}1}} & d_{1_{min}} \leq x < \chi\left(-\psi_{D_{max}}\right) \\ \frac{A_{\mathcal{C}2-2}(x)}{\Phi_{\mathcal{C}1}} & \chi\left(-\psi_{D_{max}}\right) \leq x \leq \chi\left(\psi_{D_{max}}\right), \end{cases} \tag{25}$$

where $\Phi_{\mathcal{C}1}$ is defined in (12) and

$$f_{D_1}(x) = \begin{cases} \frac{2r_D x}{r_S\left(d_{2_{max}}^2 - d_{1_{min}}^2\right)} & d_{1_{min}} \leq x < \chi\left(-\psi_{D_{max}}\right) \\ \frac{r_D \mathcal{P}(x)}{\pi r_R\left(d_{2_{max}}^2 - d_{2_{min}}^2\right)} & \chi\left(-\psi_{D_{max}}\right) \leq x \leq \chi\left(\psi_{D_{max}}\right) \end{cases}, \tag{26}$$

where $\chi(.)$ and $\mathcal{P}(.)$ are defined in (10) and (22), respectively.

D. STATE $\mathcal{D}$: $\beta_D > \psi_{D_{MAX}} - \psi_{S_{MAX}}$ AND $\beta_D > \psi_{S_{MAX}} - \psi_{D_{MAX}}$

In this section, we check the latest possible situation on the network. This situation is such that the two caps related to the source and destination overlap, but none of them is inside the other. For this reason, the entire area of the space where a relay can be selected will be different from the previous modes. Fig. 5 shows an example of the network in this state.

$$\Pi_1(d) = \frac{r_R g_1(d)}{\sqrt{g_2(d)\left(r_R^2 - g_2(d)\right)}} \cos^{-1}\left(\sqrt{r_R^2 - d_{2_{max}}^2\cos^2(\theta_D)}\csc(\beta_D) - \sqrt{r_R^2 - g_2(d)}\cot(\beta_D)\right) \tag{17}$$

$$\Pi_2(d) = \frac{r_R^2 g_1(d)}{g_2(d)} \frac{g_2(d)\frac{\sqrt{r_R^2 - d_{2_{max}}^2\cos^2(\theta_D)}}{\sqrt{r_R^2 - g_2(d)}} + \sqrt{r_R^2 - d_{2_{max}}^2\cos^2(\theta_D)}\sqrt{r_R^2 - g_2(d)} - r_R^2\cos(\beta_D)}{\sqrt{g_2(d)d_{2_{max}}^2\cos^2(\theta_D) - \left(r_R^2\cos(\beta_D) - \sqrt{r_R^2 - d_{2_{max}}^2\cos^2(\theta_D)}\sqrt{r_R^2 - g_2(d)}\right)^2}} \tag{18}$$

$$\Pi_3(d) = \frac{r_R g_1(d)}{\sqrt{g_2(d)}}\left(\cot(\beta_D) + \frac{r_R^2 - g_2(d)}{g_2(d)}\cot(\beta_D) - \frac{\sqrt{r_R^2 - g_2(d)}\sqrt{r_R^2 - d_{2_{max}}^2\cos^2(\theta_D)}}{g_2(d)}\csc(\beta_D)\right) \tag{19}$$

$$\Pi_4(d) = \sqrt{1 - \left(\frac{\sqrt{r_R^2 - d_{2_{max}}^2\cos^2(\theta_D)}}{\sqrt{g_2(d)}}\csc(\beta_D) - \frac{\sqrt{r_R^2 - g_2(d)}}{\sqrt{g_2(d)}}\cot(\beta_D)\right)^2} \tag{20}$$

$$\Pi_5(d) = r_R g_1(d) \frac{\sqrt{r_R^2 - d_{2_{max}}^2\cos^2(\theta_D)}\csc(\beta_D)}{\sqrt{r_R^2 - g_2(d)}\sqrt{d_{2_{max}}^2\cos^2(\theta_D) - \left(\sqrt{r_R^2 - g_2(d)}\csc(\beta_D) - \sqrt{r_R^2 - d_{2_{max}}^2\cos^2(\theta_D)}\cot(\beta_D)\right)^2}} \tag{21}$$

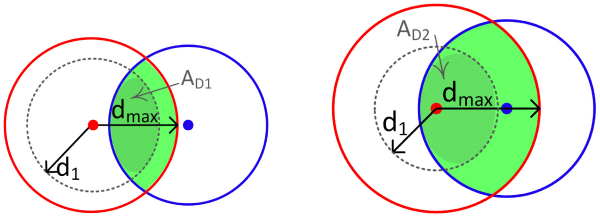

(a) State $\mathcal{D}1$ (b) State $\mathcal{D}2$

FIGURE 5. Two-dimensional map of the region covered by the source and destination and their common area in state $\mathcal{D}$. The red dot represents the position of the source and the red circle marks where the device's field of view intersects with the surface of the relay tier sphere. Similarly, the blue dot and circle indicate the destination.

1) STATE $\mathcal{D}1$ - WHEN THERE IS NO VERTICAL COVER ON THE TIER-GROUND

To reach the CDF, we first obtain the total surface as

$$\Phi_{\mathcal{D}1} = \Lambda\big(r_R, d_{2_{max}}\cos(\theta_D), d_{1_{max}}\cos(\theta_S), \beta_D\big) \quad (27)$$

where $\Lambda(.,.,.,.)$ is defined in (14) and the intersection between the two caps when the distance is less than d_1 is equal to

$$A_{\mathcal{D}1}(d_1) = \Lambda(r_R, d_{2_{max}}\cos(\theta_D), \sqrt{d_1^2 - \frac{(r_R^2 - r_S^2 - d_1^2)^2}{4r_S^2}}, \beta_D). \quad (28)$$

Therefore, the CDF is

$$F_{D1}(x) = \frac{A_{\mathcal{D}1}(x)}{\Phi_{\mathcal{D}1}} \quad (29)$$

and the PDF is

$$f_{D1}(x) = \frac{\mathcal{P}(x)}{\Phi_{\mathcal{D}1}}, \quad (30)$$

where $\mathcal{P}(.)$ is defined in (22).

2) STATE $\mathcal{D}2$ - WHEN THERE IS A VERTICAL COVER ON THE SOURCE

In this case, if the distance is between $d_{1_{min}}$ and $\chi(-\psi_{D_{max}})$ (defined in (10)), the CDF is calculated similar to state $\mathcal{C}2$ as

$$A_{\mathcal{D}2-1}(d_1) = \frac{\pi r_R}{r_S}\left(d_1^2 - d_{1_{min}}^2\right) \quad (31)$$

and for allowed values bigger than $\chi(-\psi_{D_{max}})$, we have,

$$A_{\mathcal{D}2-2}(d_1) = \Lambda(r_R, d_{2_{max}}\cos(\theta_D), \sqrt{d_1^2 - \frac{(r_R^2 - r_S^2 - d_1^2)^2}{4r_S^2}}, \beta_D), \quad (32)$$

where $\Lambda(.,.,.,.)$ is defined in (14). Therefore, the CDF and PDF of d_1 is achieved a

$$F_{D1}(x) = \begin{cases} \frac{A_{D2-1}(x)}{\Phi_{\mathcal{D}1}} & d_{1_{min}} \le x < \chi\big(-\psi_{D_{max}}\big) \\ \frac{A_{D2-2}(x)}{\Phi_{\mathcal{D}1}} & \chi\big(-\psi_{D_{max}}\big) \le x \le d_{1_{max}} \end{cases} \quad (33)$$

and

$$f_{D1}(x) = \begin{cases} \frac{2\pi r_R x}{r_S \Phi_{\mathcal{D}1}} & d_{1_{min}} \le d_1 < \chi\big(-\psi_{D_{max}}\big) \\ \frac{\mathcal{P}(x)}{\Phi_{\mathcal{D}1}} & \chi\big(-\psi_{D_{max}}\big) \le d_1 \le d_{1_{max}} \end{cases}, \quad (34)$$

respectively, similar to (25) in state $\mathcal{C}$.

Now we have the distribution of source-to-relay distance (d_1) as

$$f_{D_1}(d_1) = \begin{cases} 0 & \text{state } \mathcal{A} \\ \text{eq. (9)} & \text{state } \mathcal{B} \\ \text{eq. (16)} & \text{state } \mathcal{C}1 \\ \text{eq. (26)} & \text{state } \mathcal{C}2 \\ \text{eq. (30)} & \text{state } \mathcal{D}1 \\ \text{eq. (34)} & \text{state } \mathcal{D}2 \end{cases} \quad (35)$$

and we can utilize it to analyze the system by the statistical behavior of d_1 in all situations. In the following, we obtain the statistical behavior of the relay-to-destination distance (d_2).

IV. STATISTICAL BEHAVIOR OF THE DISTANCE BETWEEN A RELAY AND THE DESTINATION (LINK 2)

In this section, we study the statistical characteristics of link 2. Therefore, it is crucial to consider how the cones interact with each other and determine the area they use in common, similar to the analysis in the previous case. If Link 2 is considered individually, its statistical characteristics are the same as Link 1. But when the path length of link 1 is known, link 2 can no longer cover all the possible values. As shown in the preceding section, the presence or absence of a vertical cover at the source introduces a difference. This also affects the analysis of d_2. In this section, we assume d_1 has a fixed value and use this to determine the relationship for d_2. Consider the relay position is

$$POS_R = \begin{bmatrix} r_e + d_1\cos(\alpha_R) \\ d_1\sin(\alpha_R)\cos(\beta_R) \\ d_1\sin(\alpha_R)\sin(\beta_R) \end{bmatrix}, \quad (36)$$

where α_R and β_R are relay angles. Note that the points on the surface of a sphere in three-dimensional space that satisfy the above relation have the distance of d_1 from the source. So, for all scenarios, d_2 as a function of α_R, β_R and d_1 is equal to

$$d_2(\alpha_R, \beta_R, d_1) = \Big[2r_S(d_1\cos(\alpha_R) - r_D\cos(\beta_D)) + r_D^2 + d_1^2 - 2d_1 r_D(\cos(\alpha_R)\cos(\beta_D) + r_S^2 - \cos(\beta_R)\sin(\alpha_R)\sin(\beta_D))\Big]^{0.5}. \quad (37)$$

All points on the sphere's surface (x, y, z), which are at a distance of d_1 from the source, must follow these two rules.

$$x^2 + y^2 + z^2 = r_R^2 \quad (38)$$

$$(x - r_S)^2 + y^2 + z^2 = d_1^2 \quad (39)$$

Using the above equations, we conclude that all acceptable points for x as a function of d_1 are

$$x(d_1) = \frac{r_R^2 - d_1^2 + r_S^2}{2r_S}. \tag{40}$$

If the positioning of the devices is such that there is a vertical cover on the source, for small values of d_1 that have not reached the boundary of the common area, the range of changes of β_R is between $-\pi$ to π and α_R can be obtained as follows,

$$\alpha_R = \cos^{-1}\left(\frac{x(d_1) - r_S}{d_1}\right). \tag{41}$$

As d_1 increases and the model permits the hypothetical line to reach the boundary of the common area between the source and destination, the range of β_R changes. The border of the range is the surface intersection of (38), (39), and

$$(x - r_D\cos(\beta_D))^2 + (y - r_D\sin(\beta_D))^2 + z^2 = d_{2_{max}}^2$$

as follows:

$$y_c(d_1) = \frac{r_R^2 + r_D^2 - d_{2_{max}}^2 - 2x(d_1)r_D\cos(\beta_D)}{2r_D\sin(\beta_D)}. \tag{42}$$

According to (40) and (42), we have

$$z_c(d_1) = \sqrt{r_R^2 - x(d_1)^2 - y_c(d_1)^2}.$$

The collision angle is equal to

$$\beta_c(d_1) = \tan^{-1}\left(\frac{z_c(d_1)}{y_c(d_1)}\right). \tag{43}$$

So, in this case, the new range for β_R is

$$-\beta_c(d_1) \le \beta_R \le \beta_c(d_1) \tag{44}$$

and d_2 will be achieved depend on variable d_1 in the following Lemma.

Lemma 1: The PDF of d_2 as a relay-destination distance, when d_1 is given as a source-relay distance, will obtain as

$$f_{D_2|D_1=d_1}(x) = \frac{2Bx}{\beta_c(d_1)\sqrt{B^2 - \left(A - x^2\right)^2}} \tag{45}$$

where $\beta_c(d_1)$ is in (43) and A, B are defined from (46).

Proof: By applying (40) and (41) in (37), we have

$$\begin{aligned} d_2(\beta_R, d_1) = \Bigg[& r_R^2 + r_D^2 - r_S^2 - 2r_S r_D\cos(\beta_D) \\ & + 2r_D d_1 r_S^2 - r_D\left(\frac{r_R^2 - d_1^2 - r_S^2}{r_S}\right)\cos(\beta_D) \\ & - r_D\sqrt{4d_1^2 - \left(\frac{r_R^2 - d_1^2 - r_S^2}{r_S}\right)^2}\sin(\beta_D)\cos(\beta_R)\Bigg]^{0.5} \\ \triangleq & \sqrt{A - B\cos(\beta_R)}. \end{aligned} \tag{46}$$

Then, the CDF of d_2 with the uniform distribution of β_R in (44) interval is calculated as

$$\begin{aligned} F_{D_2|D1=d_1}(x) &= \mathbb{P}\left[\sqrt{A - B\cos(\beta_R)} < x\right] \\ &= 2\mathbb{P}\left[0 < \beta_R < \cos^{-1}\left(\frac{A - x^2}{B}\right)\right] \\ &= \frac{\cos^{-1}\left(\frac{A-x^2}{B}\right)}{\beta_c(d_1)}. \end{aligned} \tag{47}$$

The PDF is obtained and the lemma is proved by the derivative on x. ■

Note that the PDF of d_2 independent of d_1 can be obtained by using $f_{D_1}(x)$ in the previous section and (45) will be obtained as

$$f_{D_2}(x) = \int_{d_{1_{min}}}^{d_{1_{max}}} f_{D_2|D1=t}(x) f_{D_1}(t)dt, \tag{48}$$

which could be achieved independently in the same way as calculating the PDF of d_1 in the previous section. Therefore, the joint distance PDF is calculated by

$$f_{D_1,D_2}(x, y) = f_{D_1}(x) f_{D_2|D_1}(y|d_1 = x), \tag{49}$$

where $f_{D_1}(x)$ is in (35) and $f_{D_2|D_1}(y|d_1 = x)$ is in (45).

V. AVERAGE PROPAGATION DELAY

In the previous sections, a comprehensive analysis of the statistical behavior of d_1 and d_2 was performed, and the correlation of d_2 with d_1 was explained. We can now determine the average delay incurred during the propagation of the signal along the specified path. The total length of the links is

$$L = d_1 + d_2,$$

therefore, the total delay is considered a random variable, denoted as

$$\tau = \frac{L}{c} = \frac{d_1 + d_2}{c}, \tag{50}$$

where c represents the speed of light. To determine its average, we employ the following expression,

$$\begin{aligned} \overline{\tau} = & \int_{d_{1_{min}}}^{d_{1_{max}}} \frac{x}{c} f_{D_1}(x)dx \\ & + \int_{d_{1_{min}}}^{d_{1_{max}}} \int_{\beta_{R_{min}}}^{\beta_{R_{max}}} \frac{d_2(\alpha_R, \beta_R, x) f_{D_1}(x)}{c\left(\beta_{R_{max}} - \beta_{R_{min}}\right)} d\beta_R dx \end{aligned} \tag{51}$$

where $f_{D_1}(x)$ represents the PDF of d_1, which can vary based on the states of the network. The second integral in equation (51) possesses a finite limit and can be accurately solved using numerical methods. It is essential to note that this integral may bifurcate into two integrals contingent upon the network's state, each having distinct upper and lower limits. A noteworthy implication of this relationship is that by considering the acceptable range in the second integral, we effectively measure the entire joint surface between the two integrals. This knowledge can efficiently simplify the

calculation of the integrals, eliminating the need for frequent verification and adjustment of the integration range during numerical computation influenced by d_1.

Corollary 1: To comprehensively analyze the entire acceptable range of d_2, its distribution function can be derived independently of d_1 and subsequently used in the equation (51). Therefore, the PDF for the distance of d_2 can be calculated similarly to $f_{D_1}(x)$. It is important to consider that the situations for d_1 may not be the same as those for d_2, so both sets of conditions and instances for this path must be examined independently. Therefore, we have,

$$\overline{\tau} = \int_{d_{1_{min}}}^{d_{1max}} \frac{x}{c} f_{D_1}(x)dx + \int_{d_{2_{min}}}^{d_{2max}} \frac{y}{c} f_{D_2}(y)dy. \tag{52}$$

VI. APPLICATION IN PERFORMANCE ANALYSIS

In this section, we provide a performance metric for the proposed system model in terms of outage capacity and ergodic rate for both DF and AF relays. First, we present the received signal and then analyze the performance of the system. The received signal at the relay node is given by

$$y_r = \sqrt{\frac{P}{d_1^{\epsilon}}} h_1 s + n_r, \tag{53}$$

where P is the transmitted power of the source, ϵ is the path loss exponent, s is the information signal of the source with unit power, h_1 is the channel between the source and a relay and n_r is the zero mean Gaussian noise with variance σ_r^2 applied at the relay node. So, the SNR at the relay is obtained as

$$\gamma_1 = \frac{P|h_1|^2}{d_1^{\epsilon}\sigma_r^2}. \tag{54}$$

A. RECEIVED SNR AT THE DESTINATION

The received signal at the destination for DF relaying is represented as follows

$$y_d^{DF} = \sqrt{\frac{\hat{P}}{d_2^{\epsilon}}} h_2 \hat{s} + n_d, \tag{55}$$

where $\hat{P}$ is the transmitted power from the relay, $\hat{s}$ is the decoded source signal, h_2 is the channel between the relay and the destination, and n_d is the total noise at the destination integrated by the noise at the relay having the variance σ_d^2. Therefore, the SNR at the destination by using the DF relay is achieved as

$$\gamma_2^{DF} = \frac{\hat{P}|h_2|^2}{d_2^{\epsilon}\sigma_d^2}. \tag{56}$$

The received signal by using the AF relay at the destination as follows,

$$y_d^{AF} = \sqrt{\frac{P\hat{P}}{d_1^{\epsilon}d_2^{\epsilon}}} G h_1 h_2 s + \sqrt{\frac{\hat{P}}{d_2^{\epsilon}}} G h_2 n_r + n_d, \tag{57}$$

where G is the AF relay gain obtained as

$$G = \frac{1}{\sqrt{\frac{P}{d_1^{\epsilon}}h_1^2 + \sigma_r^2}},$$

and $\hat{P}G^2 = 1$, then, the SNR at the destination by using the AF relay is achieved as

$$\gamma_2^{AF} = \frac{P|h_1|^2|h_2|^2}{d_1^{\epsilon}|h_2|^2\sigma_r^2 + d_1^{\epsilon}d_2^{\epsilon}\sigma_d^2}. \tag{58}$$

B. CHANNEL FADING MODEL

For the modeling of satellite channels, the shadowed-Rician fading model has been proposed in [29], which has proven its suitability in various frequency bands, e.g., UHF, L, S, and Ka bands. The PDF of channel $z = |h_i|^2$, for $i = 1, 2$ is shown as

$$f_Z(z) = Ke^{-\frac{z}{2b}} {}_1F_1(m, 1, \delta z), \tag{59}$$

where ${}_1F_1(.,.,.)$ is the confluent hyper-geometric function,

$$K = \frac{(2bm)^m}{2b(2bm+\Omega)^m}$$
$$\delta = \frac{\Omega}{2b(2bm+\Omega)}$$

with $2b$ as the average power of the scatter component, Ω as the average power of LOS component, and the Nakagami fading parameter m. The PDF and CDF were simplified and rewritten for m integer values [30] as

$$f_Z(z) = \sum_{k=0}^{m-1} A_k z^k e^{-\eta z} \tag{60}$$

$$F_Z(z) = \sum_{k=0}^{m-1} \frac{A_k}{\eta^{k+1}} \gamma(1+k, \eta z) \tag{61}$$

where

$$A_k = \frac{K(-1)^k(1-m)_k\delta^k}{(k!)^2}, \eta = \frac{m}{2b(2bm+\Omega)}$$

and $(.)_k$ is the Pochhammer symbol.

C. OUTAGE CAPACITY

The outage capacity for both DF and AF relays when the instantaneous capacity falls below a threshold is given by

$$C_{out}^{DF} = \Pr\left[\min(C_1, C_2) < C_{th}\right], \tag{62}$$

$$C_{out}^{AF} = \Pr\left[C_2 < C_{th}\right], \tag{63}$$

where C_{th} is the capacity threshold, C_1 and C_2 are the instantaneous capacities at the relay and destination nodes, respectively, given by

$$C_i = \log_2(1+\gamma_i), \quad i = 1, 2 \tag{64}$$

where γ_1 is the received SNR at the relay obtained in (54) and γ_2 is the received SNR at the destination which is achieved in (56) for DF relay and in (58) for AF relay.

The average received SNR in both links depends on the link distance, which is defined as d_1 and d_2 in previous sections. Therefore, the conditional outage capacities are

$$C_{out}^{DF} = \Pr\big[\min(C_1, C_2) < C_{th} | d_1, d_2\big], \quad (65)$$
$$C_{out}^{AF} = \Pr\big[C_2 < C_{th} | d_1, d_2\big]. \quad (66)$$

First, by considering constant distances, we obtain the outage capacity averaging on the channel fading model.

Lemma 2: The outage capacity by averaging on shadowed-Rician fading considering constant distances d_1 and d_2 is achieved for AF relay in (67), shown at the bottom of the page and for DF relay in (68), shown at the bottom of the page, where $K_v(.)$ is the modified Bessel function.

Proof: See Appendix A. ■

Lemma 3: The outage capacity over distances d_1 and d_2 for relay and destination link, obtained for DF and AF relay in limited integral range as

$$\bar{C}_{out}^{DF} = \int_{D_1}\int_{D_2} \bar{C}_O^{DF}(x,y) f_{D_1}(x) f_{D_2|D_1}(y|d_1 = x) dy dx, \quad (69)$$
$$\bar{C}_{out}^{AF} = \int_{D_1}\int_{D_2} \bar{C}_O^{AF}(x,y) f_{D_1}(x) f_{D_2|D_1}(y|d_1 = x) dy dx, \quad (70)$$

where $\bar{C}_O^{DF}$ and $\bar{C}_O^{AF}$ are calculated in (68) and (67), with the PDF $f_{D_1}(x)$ and $f_{D_2|D_1=x}(y)$ in (35) and (45), respectively. The ranges of the integrals are limited as $D_1 = (d_{1_{min}}, d_{1_{max}})$ and $D_2 = (d_{2_{min}}, d_{2_{max}})$.

Proof: The outage capacity averaged over the distances $x \triangleq d_1$ and $y \triangleq d_2$, will be calculated as follows from relations (67) and (68).

$$\bar{C}_{out}^{DF} = \int_{D_1}\int_{D_2} \bar{C}_O^{DF}(x,y) f_{D_1,D_2}(x,y) dy dx, \quad (71)$$

and

$$\bar{C}_{out}^{AF} = \int_{D_1}\int_{D_2} \bar{C}_O^{AF}(x,y) f_{D_1,D_2}(x,y) dy dx. \quad (72)$$

which the joint distance PDF is defined in (49). By replacing the outage capacities on average channel and distances PDF, the Lemma is proved. ■

Proposition 1: At high SNR of the source-relay link, $\bar{\gamma}_r = \frac{P}{\sigma_r^2}$, the outage capacity can be approximated by eq. (73), shown at the bottom of the page for AF relay and eq. (74), shown at the bottom of the page in DF relay at the top of the next page, where $K_v(.)$ is the modified Bessel function, $f_{D_1,D_2}(x,y)$ is given in (49), $D_1 = (d_{1_{min}}, d_{1_{max}})$ and $D_2 = (d_{2_{min}}, d_{2_{max}})$.

Proof: Using a similar method to obtain the outage capacity in the AF relay in the Appendix A and considering $\frac{P}{\sigma_r^2} \to \infty$, the defined parameter

$$A = \eta_1\Big(2^{C_{th}} - 1\Big)\frac{d_1^{\epsilon}\sigma_r^2}{P} \to 0,$$

then by some simplification, the outage capacity for fixed distances d_1 and d_2 by averaging on the channel is achieved. Then, we have (73) by averaging the distance distribution in (49).

In the DF relay model, when the power of the source-to-relay path approaches infinity, the performance of this link becomes optimal, and the relay can correctly decode all the received signals. As a result, the network's performance will entirely depend on the relay-to-destination path. Then, the Proposition is proved by averaging the distance distribution in (74). ■

Note that high SNR in the first link of a relay network causes the system evaluation to depend on and be limited by the performance of the second link. In the AF relay,

$$\bar{C}_O^{AF} = \sum_{k_1=0}^{m_1-1}\sum_{k_2=0}^{m_2-1} \frac{A_{k_1}A_{k_2}}{\eta_1^{k_1+1}}\Gamma(1+k_1)\Big(\eta_2^{-k_2-1}\Gamma(1+k_2) - e^{-\left(\eta_1(2^{C_{th}}-1)\frac{d_1^{\epsilon}\sigma_r^2}{P}\right)}\sum_{n_1=0}^{k_1}\sum_{n_2=0}^{n_1}\binom{n_1}{n_2}$$
$$\times \frac{1}{n_1!}\Big(\eta_1\Big(2^{C_{th}}-1\Big)\frac{d_1^{\epsilon}\sigma_r^2}{P}\Big)^{n_1-n_2} 2\Big(\eta_1(2^{C_{th}}-1)d_1^{\epsilon}d_2^{\epsilon}\sigma_d^2\Big)^{\frac{1+k_2+n_1}{2}}\eta_2^{-\frac{1+k_2-n_1}{2}} K_{n_1-1-k_2}\Big(2\sqrt{\eta_1\eta_2 d_1^{\epsilon}d_2^{\epsilon}\sigma_d^2(2^{C_{th}}-1)}\Big)\Big) \quad (67)$$

$$\bar{C}_O^{DF} = 1 - \Big(1 - F_{z_1}\Big(\frac{d_1^{\epsilon}\sigma_r^2}{P}(2^{C_{th}}-1)\Big)\Big)\Big(1 - F_{z_2}\Big(\frac{d_2^{\epsilon}\sigma_d^2}{\hat{P}}(2^{C_{th}}-1)\Big)\Big) \quad (68)$$

$$\bar{C}_{out}^{AF,high-SNR} = \int_{D_1}\int_{D_2}\sum_{k_1=0}^{m_1-1}\sum_{k_2=0}^{m_2-1}\frac{A_{k_1}A_{k_2}}{\eta_1^{k_1+1}\eta_2^{k_2+1}}\Gamma(1+k_1)\Bigg(\Gamma(1+k_2) - \sum_{n_1=0}^{k_1}\frac{2}{n_1!}\Big(\eta_1\eta_2 x^{\epsilon}y^{\epsilon}\sigma_d^2\Big(2^{C_{th}}-1\Big)\Big)^{\frac{1+k_2+n_1}{2}}$$
$$\times K_{n_1-1-k_2}\Big(2\sqrt{\eta_1\eta_2 x^{\epsilon}y^{\epsilon}\sigma_d^2(2^{C_{th}}-1)}\Big)\Bigg) f_{D_1,D_2}(x,y)dydx. \quad (73)$$

$$\bar{C}_{out}^{DF,high-SNR} = \int_{D_1}\int_{D_2}\sum_{k_2=0}^{m_2-1}\frac{A_{k_2}}{\eta^{k_2+1}}\gamma\Big(1+k_2, \eta\frac{y^{\epsilon}\sigma_d^2}{\hat{P}}\Big(2^{C_{th}}-1\Big)\Big) f_{D_1,D_2}(x,y)dydx. \quad (74)$$

amplifying the signal when the first link has a high SNR, G depends on the received signal power from the source in our system design decreases.

D. ERGODIC RATE

The ergodic rate, or ergodic capacity, provides a measure of the average data rate that can be achieved over a communication channel when the channel conditions vary over time. Here is the ergodic rate for both AF and DF relay systems as

$$\bar{R}^{DF} = \mathbb{E}\big[\log_2(1+\min\big(\gamma_1, \gamma_2^{DF}\big)\big], \tag{75}$$

$$\bar{R}^{AF} = \mathbb{E}\big[\log_2\big(1+\gamma_2^{AF}\big)\big], \tag{76}$$

where γ_1, γ_2^{DF} and γ_2^{AF} are defined in (54), (56), and (58), respectively.

The ergodic rate for the DF relay achieves by definition a new random variable as $W = \min(\gamma_1, \gamma_2^{DF})$ and averaging on that. To obtain the PDF of the minimum of two variables we should derivate the CDF of the minimum which is calculated as

$$F_W(w) = F_{\gamma_1}(w) + F_{\gamma_2^{DF}}(w) - F_{\gamma_1}(w)F_{\gamma_2^{DF}}(w), \tag{77}$$

then $f_W(w) = \frac{dF_W(w)}{dw}$ is obtained as

$$\begin{aligned} f_W(w) = {} & f_{\gamma_1}(w) + f_{\gamma_2^{DF}}(w) - f_{\gamma_1}(w)F_{\gamma_2^{DF}}(w) \\ & - F_{\gamma_1}(w)f_{\gamma_2^{DF}}(w) \end{aligned} \tag{78}$$

where

$$f_{\gamma_1}(w) = \frac{d_1^{\epsilon}\sigma_r^2}{P}\sum_{k_1=0}^{m_1-1} A_{k_1}\left(\frac{d_1^{\epsilon}\sigma_r^2}{P}w\right)^{k_1} e^{-\eta_1\left(\frac{d_1^{\epsilon}\sigma_r^2}{P}w\right)} \tag{79}$$

$$F_{\gamma_1}(w) = \sum_{k_1=0}^{m_1-1}\frac{A_{k_1}}{\eta_1^{k_1+1}}\gamma\left(1+k_1, \eta_1\frac{d_1^{\epsilon}\sigma_r^2}{P}w\right) \tag{80}$$

and

$$f_{\gamma_2^{DF}}(w) = \frac{d_2^{\epsilon}\sigma_d^2}{\hat{P}}\sum_{k_2=0}^{m_2-1} A_{k_2}\left(\frac{d_2^{\epsilon}\sigma_d^2}{\hat{P}}w\right)^{k_2} e^{-\eta_2\left(\frac{d_2^{\epsilon}\sigma_d^2}{\hat{P}}w\right)} \tag{81}$$

$$F_{\gamma_2^{DF}}(w) = \sum_{k_2=0}^{m_2-1}\frac{A_{k_2}}{\eta_2^{k+1}}\gamma\left(1+k_2, \eta_2\frac{d_2^{\epsilon}\sigma_d^2}{\hat{P}}w\right), \tag{82}$$

so, the ergodic rate for DF relay achieves as

$$\begin{aligned} \bar{R}^{DF} = {} & \int_{D_1}\int_{D_2}\int_0^{\infty}\log_2(1+w)f_W(w)dw \\ & \times f_{D_1}(x)f_{D_2|D_1}(y|d_1=x)dydx. \end{aligned} \tag{83}$$

The ergodic rate for the AF relay achieves by replacing (58) in (76) and averaging on channel fading $z_1 \triangleq h_1^2$ and $z_2 \triangleq h_2^2$ from (60).

The ergodic rate in this paper is calculated by taking the Taylor expansion and retaining up to its second order with reference to [31, eq. (22)] as

$$\bar{R} = \mathbb{E}\big[\log_2(1+\gamma)\big] = \frac{1}{\ln(2)}\mathbb{E}\big[\ln(1+\gamma)\big] \tag{84}$$

$$\approx \frac{\ln\big(1+\mathbb{E}[\gamma]\big)}{\ln(2)} - \frac{\mathbb{E}\big[\gamma^2\big]-\big(\mathbb{E}[\gamma]\big)^2}{2\ln(2)\big(1+\mathbb{E}[\gamma]\big)^2}. \tag{85}$$

Another method for calculating the ergodic rate is to use [32, eq. (28)], which can be applied to the CDF from (77). The ergodic rate is obtained in the following Lemma.

Lemma 4: The ergodic rate over shadowed-Rician fading and averaging on random distances $d_1 = x$ and $d_2 = y$ for DF and AF relay is achieved as

$$\begin{aligned} \bar{R}^{DF} = {} & \int_{D_1}\int_{D_2}\frac{1}{2}\left(\frac{\ln(1+\mathbb{E}[w])}{\ln(2)} - \frac{\mathbb{E}\big[w^2\big]-(\mathbb{E}[w])^2}{2\ln(2)(1+\mathbb{E}[w])^2}\right) \\ & \times f_{D_1,D_2}(x,y)dydx. \end{aligned} \tag{86}$$

where $w = \gamma_2^{AF}$ and

$$\begin{aligned} \bar{R}^{AF} = {} & \int_{D_1}\int_{D_2}\frac{1}{2}\left(\frac{\ln\big(1+\mathbb{E}\big[\gamma_2^{AF}\big]\big)}{\ln(2)} - \frac{\mathbb{E}\big[\gamma_2^{AF2}\big]-\big(\mathbb{E}\big[\gamma_2^{AF}\big]\big)^2}{2\ln(2)\big(1+\mathbb{E}\big[\gamma_2^{AF}\big]\big)^2}\right) \\ & \times f_{D_1,D_2}(x,y)dydx, \end{aligned} \tag{87}$$

respectively, $f_{D_1,D_2}(x,y)$ is defined in (49), the ranges of the integrals are limited as $D_1 = (d_{1_{min}}, d_{1_{max}})$, $D_2 = (d_{2_{min}}, d_{2_{max}})$ and a factor of $\frac{1}{2}$ is introduced because the end-to-end communication is established by means of two successive phases of transmission.

Proof: See Appendix B. ∎

Proposition 2: At high SNR of the source-relay link, $\bar{\gamma}_r = \frac{P}{\sigma_r^2} \to \infty$, the ergodic capacity for DF relay is achieved as

$$\begin{aligned} \bar{R}^{DF,high-SNR} = {} & \int_{D_1}\int_{D_2}\frac{1}{2}\left(\frac{\ln\big(1+\mathbb{E}\big[w^{high-SNR}\big]\big)}{\ln(2)} - \right. \\ & \left.\frac{\mathbb{E}\Big[\big(w^{high-SNR}\big)^2\Big]-\Big(\mathbb{E}\big[w^{high-SNR}\big]\Big)^2}{2\ln(2)\big(1+\mathbb{E}\big[w^{high-SNR}\big]\big)^2}\right)f_{D_1,D_2}(x,y)dydx \end{aligned} \tag{88}$$

where $\mathbb{E}[w^{high-SNR}] = I_2'$ and $\mathbb{E}[(w^{high-SNR})^2] = I_2''$ and I_2' and I_2'' are defined in (106) and (110), respectively, and for AF relay achieves as

$$\begin{aligned} \bar{R}^{AF,high-SNR} = {} & \int_{D_1}\int_{D_2}\frac{1}{2}\left(\frac{\ln\big(1+\mathbb{E}\big[\gamma^{high-SNR}\big]\big)}{\ln(2)}\right. \\ & \left. - \frac{\mathbb{E}\Big[\big(\gamma^{high-SNR}\big)^2\Big]-\Big(\mathbb{E}\big[\gamma^{high-SNR}\big]\Big)^2}{2\ln(2)\big(1+\mathbb{E}\big[\gamma^{high-SNR}\big]\big)^2}\right)f_{D_1,D_2}(x,y)dydx \end{aligned} \tag{89}$$

where $\mathbb{E}[\gamma^{high-SNR}]$ and $\mathbb{E}[(\gamma^{high-SNR})^2]$ are calculated in (90) and (91), respectively. For both DF and AF relay, $f_{D_1,D_2}(x,y)$ is defined in (49).

Proof: From (86), given the large value of γ_1, the term $w^{\text{high-SNR}} = \min(\gamma_1, \gamma_2^{DF})$ simplifies to $w^{\text{high-SNR}} = \gamma_2^{DF}$. As a result, the distribution function of w simplifies to the distribution function of γ_2^{DF} and $\bar{R}^{DF,high-SNR}$ is achieved.

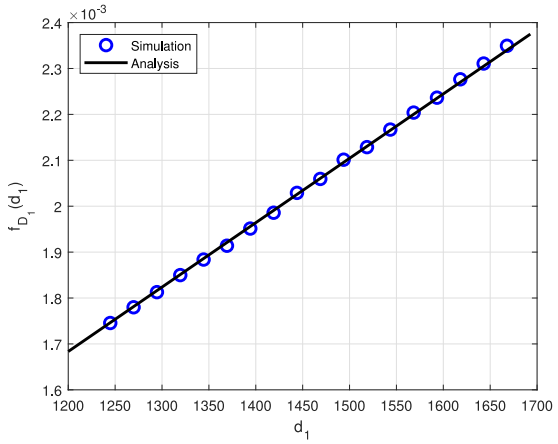

FIGURE 6. Simulation and analysis of PDF of d_1 in the state $\mathcal{B}$ where $\theta_S = 40°$, $\beta_D = 2°$, and $\theta_D = 20°$.

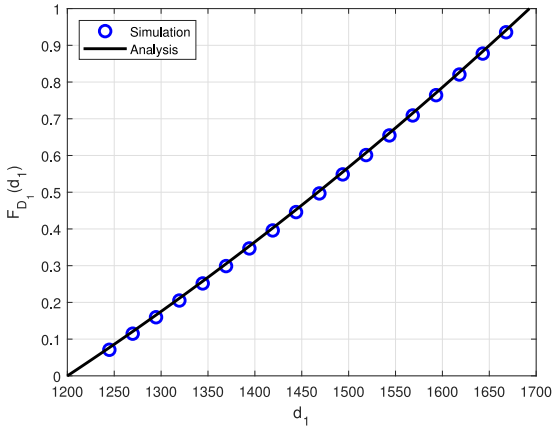

FIGURE 7. Simulation and analysis of CDF of d_1 in the state $\mathcal{B}$ where $\theta_S = 40°$, $\beta_D = 2°$, and $\theta_D = 20°$.

For AF relay, (115) will be updated and solved as

$$\mathbb{E}\left[\gamma^{high-SNR}\right] = P \sum_{k_1=0}^{m_1-1} \sum_{k_2=0}^{m_2-1} \frac{A_{k_1} A_{k_2}}{x^{\epsilon} y^{\epsilon} \sigma_d^2 \eta_1^{k_1+2} \eta_2^{k_2+2}} \times \Gamma(k_1+2)\Gamma(k_2+2), \quad (90)$$

and the second order from (119) is updated as

$$\mathbb{E}\left[\left(\gamma^{high-SNR}\right)^2\right] = P^2 \sum_{k_1=0}^{m_1-1} \sum_{k_2=0}^{m_2-1} \frac{A_{k_1} A_{k_2}}{\eta_1^{k_1+3} \eta_2^{k_2+3} \left(x^{\epsilon} y^{\epsilon} \sigma_d^2\right)^2} \times \Gamma(k_1+3)\Gamma(k_2+3). \quad (91)$$

By substituting the first and second-order expectation values, the proposition is proven. ■

VII. SIMULATION AND NUMERICAL RESULTS

In this section, we utilize the derived formulas to validate the behavior of distances under various conditions and to assess their performance. Monte Carlo simulations, consisting of 10^7 iterations, were conducted using MATLAB. The devices located in tier-space are positioned 1200 km above the Earth, while those in tier-air are 10 km above the surface. The parameters for channel fading and the system model used to plot the outage capacity and ergodic rate in Scenario I are as follows: $m_1 = 5$, $m_2 = 2$, $\sigma_r^2 = \sigma_d^2 = 0.001$, $\epsilon = 1.2$ and $P = 10^5$.

Figs. 6-11 show the statistical behavior of the first link distance, d_1, for different states that came in (35). We consider scenario I, where the relay and destination devices are placed on the space and air tiers, respectively. It is assumed that the device on tier-air is at an altitude of $r_D - r_S = 10$km above the earth's surface with an angle of β_D and a field of view of θ_D, where the field of view of the device on tier-ground is called θ_S.

Figs. 6 and 7 show the PDF and CDF of the distance between tier-ground and tier-space (d_1). This figure was obtained for a situation where the field of view of the device on tier-ground is completely inside the device on tier-air and the network is in state $\mathcal{B}$. It is assumed that the device on tier-air is at an angle of $\beta_D = 2°$ and a field of view of $\theta_D = 20°$, and the field of view of the device on the ground is $\theta_S = 40°$. The simulation results are confirmed by our obtained analytical expression.

Figs. 8 and 9 show the PDF and CDF of the distance d_1 for a situation where the field of view of the device on tier-air is completely inside the device on tier-ground, but the network is in states $\mathcal{C}1$ and $\mathcal{C}2$. For state $\mathcal{C}1$, the device on tier-air is assumed to be at an angle of $\beta_D = 8°$ and $\theta_D = 50°$, and the field of view of the device on tier-ground is $\theta_S = 20°$. For state $\mathcal{C}2$, it is assumed that $\beta_D = 5°$ and $\theta_D = 35°$, and the field of view of tier-ground is $\theta_S = 20°$. As expected, the simulation results are confirmed by our obtained analytical expression. In contrast to the previous case, according to Fig. 8, the distance is more likely to be closer to the value of $d_{1_{min}}$ than to the state $\mathcal{B}$. The change in direction of the graph for state $\mathcal{C}2$ is due to the two rules of the distribution function in (26). This graph can be viewed as a combination of the two states $\mathcal{B}$ and $\mathcal{C}1$. In the initial part of the curve, the PDF graph resembles the state $\mathcal{B}$, and later it resembles $\mathcal{C}1$.

Figs. 10 and 11 show the PDF and CDF of d_1, where the fields of view of devices on tier-ground and tier-air have a common area and the network is in states $\mathcal{D}1$ and $\mathcal{D}2$. For state $\mathcal{D}1$ it is assumed that $\beta_D = 20°$, $\theta_D = 20°$, and $\theta_S = 30°$, and for the state $\mathcal{D}2$ it is assumed that $\beta_D = 10°$, $\theta_D = 20°$, and $\theta_S = 20°$. As expected, the analysis and simulation results verify each other. This diagram can be seen as a combination of the states $\mathcal{B}$ and $\mathcal{D}1$. In its initial part of the curve, the PDF diagram resembles the state $\mathcal{B}$, and later it resembles $\mathcal{D}1$.

Fig. 12 shows the average signal delay in the network versus β_D, which represents the position of the device on tier-air. Three different modes of this network are shown, and the viewing angles of the devices on tier-air and tier-ground $[\theta_D, \theta_S]$ have different values as [20°,15°], [20°,20°], and [30°,20°]. In general, as you can see in the figure,

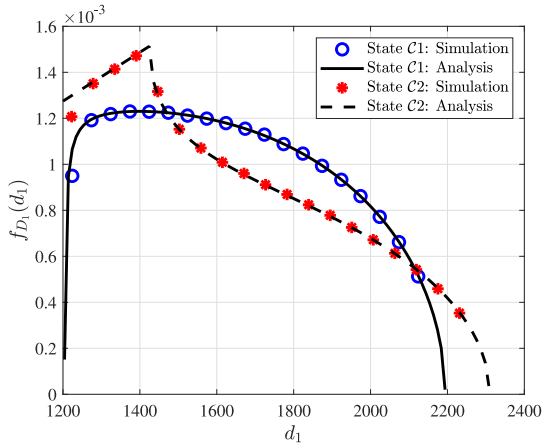

FIGURE 8. Simulation and analysis of PDF of d_1 in the state $\mathcal{C}$ where $\theta_S = 20°$, $\beta_D = 8°$, $\theta_D = 50°$ for $\mathcal{C}1$ and $\beta_D = 5°$, $\theta_D = 35°$ for $\mathcal{C}2$.

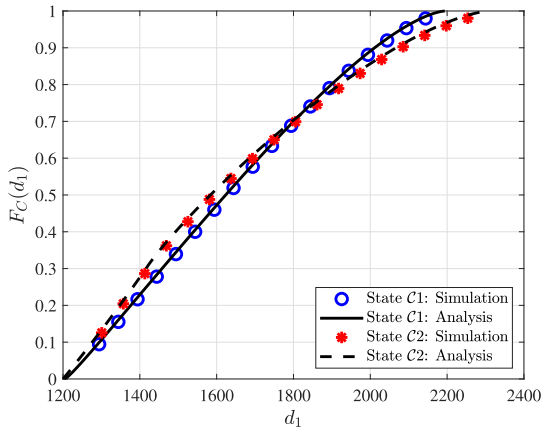

FIGURE 9. Simulation and analysis of CDF of d_1 in the state $\mathcal{C}$ where $\theta_S = 20°$, $\beta_D = 8°$, $\theta_D = 50°$ for $\mathcal{C}1$ and $\beta_D = 5°$, $\theta_D = 35°$ for $\mathcal{C}2$.

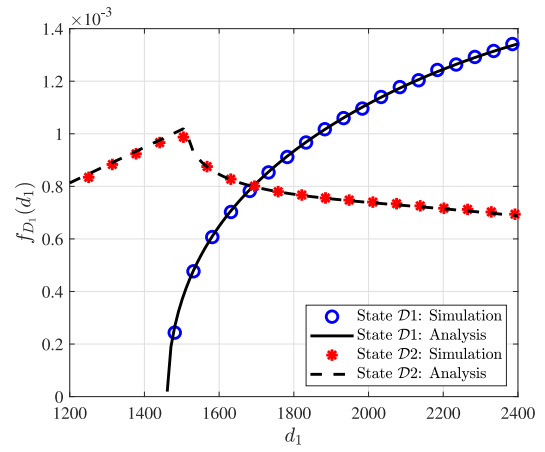

FIGURE 10. Simulation and analysis of PDF of d_1 in the state $\mathcal{D}$ where $\theta_S = 30°$, $\beta_D = 20°$, $\theta_D = 20°$ for $\mathcal{D}1$ and $\beta_D = 10°$ and $\theta_D = 20°$ for $\mathcal{D}2$.

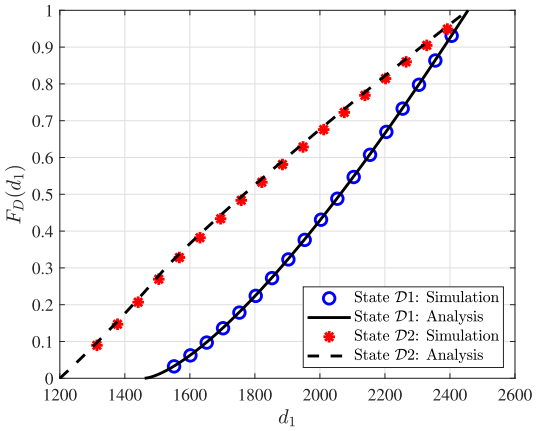

FIGURE 11. Simulation and analysis of CDF of d_1 in the state $\mathcal{D}$ where $\theta_S = 30°$, $\beta_D = 20°$, $\theta_D = 20°$ for $\mathcal{D}1$ and $\beta_D = 10°$ and $\theta_D = 20°$ for $\mathcal{D}2$.

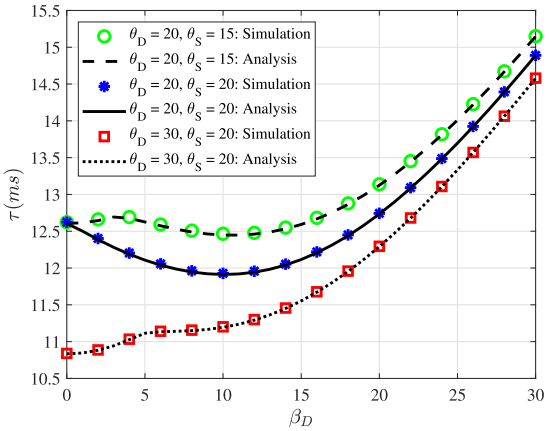

FIGURE 12. The total average delay propagation versus β_D.

based on the device's position on tier-air, the average delay increases as the device moves away (larger β_D). However, there is a small decrease and also a minimum in some cases, which is reasonable due to the change of the distances of the common area (green area) on tier-air by changing β_D. For example, when β_D changes from 5° to 10°, the average delay decreases, and we also have a minimum average delay at $\beta_D = 10°$ when $\theta_S = \theta_D = 20°$.

Figs. 13 and 14 depict the performance evaluation of applying distance distribution to relay systems. Fig. 13 shows the outage capacity vs. capacity threshold (C_{th}), which experiences different states based on the location of the source and destination. The parameters $\theta_S = 40°$, $\theta_D = 20°$, and $\beta_D = 2°$ correspond to state $\mathcal{B}$, while $\theta_S = 30°$, $\theta_D = 20°$, and $\beta_D = 20°$ correspond to state $\mathcal{D}1$, where the distance distribution function for these two states differs. As a result, we observe their impact on the outage capacity for both AF and DF relays. The outage capacity is plotted numerically from (71) and (72) by averaging over both fading channels and both distances of links 1 and 2.

Fig. 14 shows the outage capacity vs. the first link as a source-relay SNR ($\bar{\gamma}_r = \frac{P}{\sigma_r^2}$) for AF and DF relays. Increasing the SNR in the first link improves the outage capacity in both relays, but they behave differently. The improvement in the DF relay is greater than in the AF relay because the SNR in the first link plays a more important role

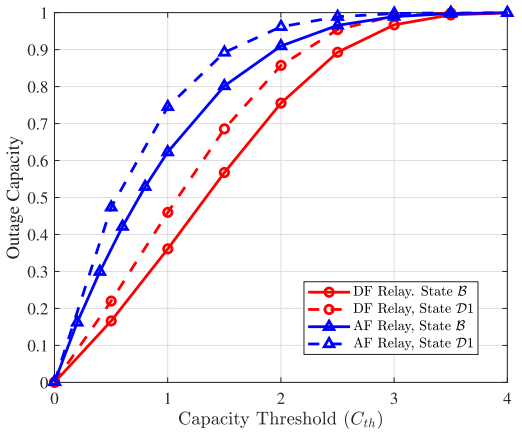

FIGURE 13. The outage capacity versus capacity threshold for AF and DF relay.

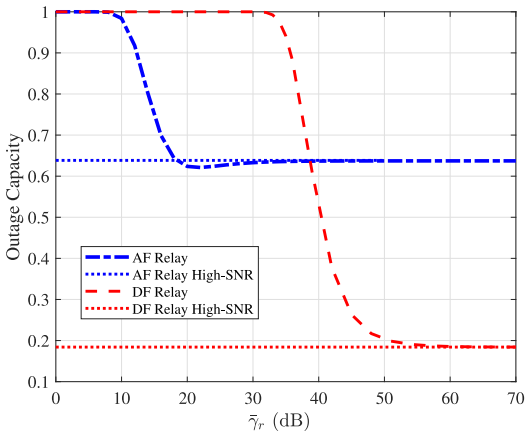

FIGURE 14. The outage capacity versus the average SNR of the first link (source-relay) where $\bar{\gamma}_r = \frac{P}{\sigma_r^2}$ for both AF and DF relay and $C_{th} = 1$.

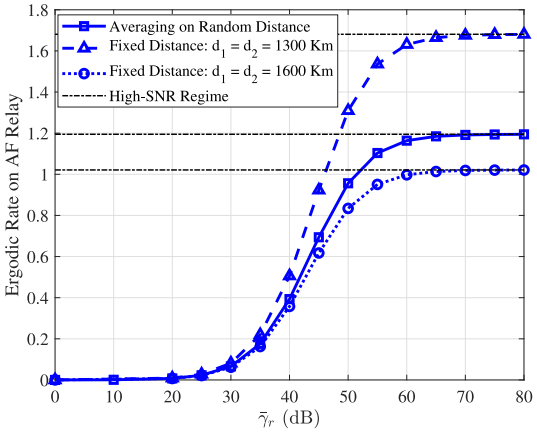

FIGURE 15. The ergodic rate versus the average SNR of the first link (source-relay) in AF relay.

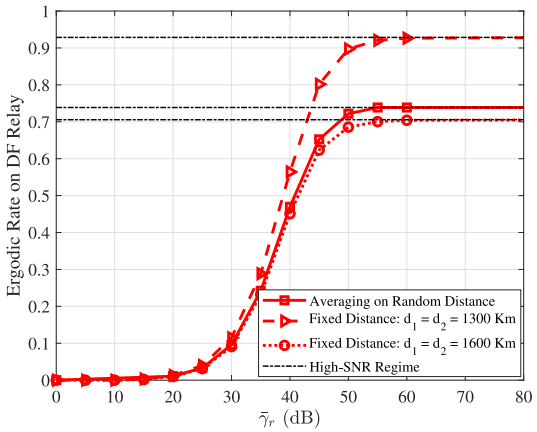

FIGURE 16. The ergodic rate versus the average SNR of the first link (source-relay) in DF relay.

in decoding, while the second link also plays an effective role in amplifying. The figure is also plotted for a high SNR regime, illustrating the limitation when the SNR of the first link is significantly large. Thus, it is not possible to reduce the outage capacity in a system by more than a certain probability.

Figs. 15 and 16 illustrate the ergodic rate for AF and DF relays, respectively, plotted as a function of the average SNR in the first link where $\bar{\gamma}_r = \frac{P}{\sigma_r^2}$ for Scenario I. As the SNR increases, the ergodic rate improves; however, this increase eventually stabilizes due to the limitation of the second link. In both figures, the average rate is computed over varying distances and compared to the case where the distances in the first and second links are considered fixed. The distance distribution varies according to the position and angle of the devices, and for all possible configurations, the distance distribution–which is the primary focus of this paper–has been derived.

Fig. 15 shows the difference in the ergodic rate for the AF relay when the assumed distance is either shorter (1300 Km) or longer (1600 Km) than the actual distance. This highlights the importance of accurately determining the distance distribution for more precise system analysis. Similarly, Fig. 16 demonstrates this performance variation for the DF relay. Furthermore, in Figs. 15 and 16, the asymptotic average rate for high SNR is plotted based on Proposition 2.

Note that our results are given for scenario I, when the source is in tier-ground and the destination is in tier-air, so the relay should be in a green area of tier-space. Having the location and angles of view of the source and destination gives us the possible area to have a relay on it, which is called the green area (Fig. 1(a)). On the other hand, in Scenario II, when the source is in the tier-ground and the destination is in the tier-space, the relay will be in a green area of the tier-air. Thus, the boundary of the green area can be found based on the position and angle of view of the source and destination in the same way as in Scenario I. Therefore, for Scenario II, we can know the statistical distribution of distances. In whatever scenario we are in, the distance of the first link between the source and the relay is d_1 and the distance of the second link between the relay and the destination is d_2. The distribution function of d_1 and d_2 is calculated based on their tiers, which are analyzed in

Section III, and the simulation method has no difference in Scenarios I and II.

VIII. CONCLUSION

The study presented in this paper highlights the intricate relationship between device placement and the corresponding signal propagation in a multi-layer 3D network such as Non-Terrestrial Networks. By formulating comprehensive closed-form equations that consider the spherical geometry of the problem, we were able to investigate the various statistical implications of different device locations. Our analysis encompassed two different scenarios, allowing us to quantify the average signal propagation delay, outage capacity, and ergodic rate across the network in both AF and DF relays.

The results underscore the need for careful tuning of network power and performance parameters when deploying a multi-tier system. This is critical to ensure the desired performance levels given the various distance and link length conditions that significantly affect the distribution of signal propagation. The analysis is validated with comprehensive Monte Carlo evaluations. Our research demonstrates the critical role that the average signal propagation delay plays and highlights its profound impact on network parameters under various device placement and radiation assumptions. This serves as a fundamental guide for future network design and optimization, emphasizing the importance of considering distance-related factors to achieve optimal performance and reliability. Future work includes the study of hybrid AF/DF relays which can automatically select the most suitable cooperative diversity protocol (AF or DF) for each time instant. Another avenue of future work is the extension of the delay study by analyzing other metrics such as the Age of Information (AoI), for which the queueing processes of the multi-hop relay network must be considered.

APPENDIX A
PROOF OF OUTAGE CAPACITY

The proof of outage capacity for AF and DF relays is presented below:

A.AF RELAY

For AF relay, we have

$$\bar{C}_O^{AF} = \Pr\left[\log_2\left(1+\frac{P|h_1|^2|h_2|^2}{d_1^{\epsilon}|h_2|^2\sigma_r^2+d_1^{\epsilon}d_2^{\epsilon}\sigma_d^2}\right) < C_{th}\right] = \Pr\left[|h_1|^2 < \left(2^{C_{th}}-1\right)\left(\frac{d_1^{\epsilon}\sigma_r^2}{P}+\frac{d_1^{\epsilon}d_2^{\epsilon}\sigma_d^2}{P|h_2|^2}\right)\right] \quad (92)$$

by using $z_1 \triangleq |h_1|^2$ and $z_2 \triangleq |h_2|^2$, we have

$$\bar{C}_O^{AF} = \int_0^{\infty} F_{Z_1}\left((2^{C_{th}}-1)\left(\frac{d_1^{\epsilon}\sigma_r^2}{P}+\frac{d_1^{\epsilon}d_2^{\epsilon}\sigma_d^2}{Pz_2}\right)\right) f_{Z_2}(z_2)dz_2$$

by replacing the PDF and CDF of the shadowed-Rician model in (60) and (61), we have

$$\bar{C}_O^{AF} = \int_0^{\infty} \sum_{k_1=0}^{m_1-1} \frac{A_{k_1}}{\eta_1^{k_1+1}} \gamma\left(1+k_1, A+\frac{B}{z_2}\right) \times \sum_{k_2=0}^{m_2-1} A_{k_2} z_2^{k_2} e^{-\eta_2 z_2} dz_2, \quad (93)$$

where $A = \eta_1(2^{C_{th}}-1)\frac{d_1^{\epsilon}\sigma_r^2}{P}$, $B = \eta_1(2^{C_{th}}-1)d_1^{\epsilon}d_2^{\epsilon}\sigma_d^2$. To solve the integral, we expand Gamma incomplete from [33, 8.352.6] as

$$\gamma\left(1+k_1, A+\frac{B}{z_2}\right) = \Gamma(1+k_1) \times \left(1-e^{-\left(A+\frac{B}{z_2}\right)}\sum_{n=0}^{k_1}\frac{1}{n!}\left(A+\frac{B}{z_2}\right)^n\right) \quad (94)$$

and use Binomial series as

$$\gamma\left(1+k_1, A+\frac{B}{z_2}\right) = \Gamma(1+k_1)\left(1-e^{-\left(A+\frac{B}{z_2}\right)} \sum_{n_1=0}^{k_1}\sum_{n_2=0}^{n_1}\frac{1}{n_1!}\binom{n_1}{n_2}\left(\frac{B}{z_2}\right)^{n_1} A^{n_1-n_2}\right). \quad (95)$$

Now, the outage capacity for the AF relay is achieved as

$$\bar{C}_O^{AF} = \sum_{k_1=0}^{m_1-1}\sum_{k_2=0}^{m_2-1} A_{k_2}\frac{A_{k_1}}{\eta_1^{k_1+1}}\Gamma(1+k_1)(I_1-I_2)$$

where

$$I_1 = \int_0^{\infty} z_2^{k_2} e^{-\eta_2 z_2} dz_2 = \eta_2^{-k_2-1}\Gamma(1+k_2) \quad (96)$$

$$I_2 = e^{-A}\sum_{n_1=0}^{k_1}\sum_{n_2=0}^{n_1}\binom{n_1}{n_2}\frac{B^{n_1}A^{n_1-n_2}}{n_1!} \times \int_0^{\infty} z_2^{k_2-n_1} e^{-\eta_2 z_2-\frac{B}{z_2}} dz_2, \quad (97)$$

$$= e^{-A}\sum_{n_1=0}^{k_1}\sum_{n_2=0}^{n_1}\binom{n_1}{n_2}\frac{B^{n_1}A^{n_1-n_2}}{n_1!} 2\left(\frac{B}{\eta_2}\right)^{\frac{1+k_2-n_1}{2}} \times K_{n_1-1-k_2}\left(2\sqrt{B\eta_2}\right). \quad (98)$$

Finally, outage capacity in closed form is obtained as

$$\bar{C}_O^{AF} = \sum_{k_1=0}^{m_1-1}\sum_{k_2=0}^{m_2-1} A_{k_2}\frac{A_{k_1}}{\eta_1^{k_1+1}}\Gamma(1+k_1) \times \left(\eta_2^{-k_2-1}\Gamma(1+k_2) - e^{-A}\sum_{n_1=0}^{k_1}\sum_{n_2=0}^{n_1}\binom{n_1}{n_2}\frac{B^{n_1}A^{n_1-n_2}}{n_1!} \times 2\left(\frac{B}{\eta_2}\right)^{\frac{1+k_2-n_1}{2}} K_{n_1-1-k_2}\left(2\sqrt{B\eta_2}\right)\right) \quad (99)$$

By replacing A and B, the outage capacity for AF relay is in (67).

B.DF RELAY

The outage capacity by averaging on the channel model for the DF relay is calculated as

$$\begin{aligned}\bar{C}_O^{DF} &= \Pr\left[\min\left(\log_2\left(1+\frac{P|h_1|^2}{d_1^{\epsilon}\sigma_r^2}\right),\log_2\left(1+\frac{\hat{P}|h_2|^2}{d_2^{\epsilon}\sigma_d^2}\right)\right) < C_{th}\right] \\ &= 1-\underbrace{\Pr\left(\log_2(1+\frac{P|h_1|^2}{d_1^{\epsilon}\sigma_r^2}) \geq C_{th}\right)}_{P_1} \\ &\quad \times \underbrace{\Pr\left(\log_2(1+\frac{\hat{P}|h_2|^2}{d_2^{\epsilon}\sigma_d^2}) \geq C_{th}\right)}_{P_2}. \end{aligned} \tag{100}$$

Above probabilities by using $z_1 \triangleq h_1^2$ and $z_2 \triangleq h_2^2$, obtain as

$$\begin{aligned} P_1 &= \Pr\left(z_1 \geq \frac{d_1^{\epsilon}\sigma_r^2}{P}(2^{C_{th}}-1)\right) \\ &= 1-F_{z_1}\left(\frac{d_1^{\epsilon}\sigma_r^2}{P}(2^{C_{th}}-1)\right) \end{aligned} \tag{101}$$

and

$$\begin{aligned} P_2 &= \Pr\left(z_2 \geq \frac{d_2^{\epsilon}\sigma_d^2}{\hat{P}}(2^{C_{th}}-1)\right) \\ &= 1-F_{z_2}\left(\frac{d_2^{\epsilon}\sigma_d^2}{\hat{P}}(2^{C_{th}}-1)\right) \end{aligned} \tag{102}$$

Finally by replacing the CDF of the shadowed-Rician channel (61), the outage capacity in the DF relay is achieved in (68).

APPENDIX B
PROOF OF ERGODIC RATE FOR AF RELAY

The proof of the ergodic rate for AF and DF relays is presented below:

A.DF RELAY

The first and second moments of w are calculating as

$$\begin{aligned}\mathbb{E}[w] &= \underbrace{\int_0^{\infty} w f_{\gamma_1}(w)}_{I_1'} + \underbrace{\int_0^{\infty} w f_{\gamma_2^{DF}}(w)dw}_{I_2'} \\ &\quad - \underbrace{\int_0^{\infty} w f_{\gamma_1}(w)F_{\gamma_2^{DF}}(w)dw}_{I_3'} - \underbrace{\int_0^{\infty} w F_{\gamma_1}(w) f_{\gamma_2^{DF}}(w)dw}_{I_4'} \end{aligned} \tag{103}$$

and

$$\begin{aligned}\mathbb{E}\left[w^2\right] &= \underbrace{\int_0^{\infty} w^2 f_{\gamma_1}(w)}_{I_1''} + \underbrace{\int_0^{\infty} w^2 f_{\gamma_2^{DF}}(w)dw}_{I_2''} \\ &\quad - \underbrace{\int_0^{\infty} w^2 f_{\gamma_1}(w)F_{\gamma_2^{DF}}(w)dw}_{I_3''} - \underbrace{\int_0^{\infty} w^2 F_{\gamma_1}(w) f_{\gamma_2^{DF}}(w)dw}_{I_4''}. \end{aligned} \tag{104}$$

Both moments break down into four integrals. We have the solutions for the integrals using the PDF and CDF in (79)-(82) as

$$I_1' = \frac{P}{d_1^{\epsilon}\sigma_r^2}\sum_{k_1=0}^{m_1-1}\frac{A_{k_1}}{\eta_1^{k_1+2}}\Gamma(k_1+2), \tag{105}$$

$$I_2' = \frac{\hat{P}}{d_2^{\epsilon}\sigma_d^2}\sum_{k_2=0}^{m_2-1}\frac{A_{k_2}}{\eta_2^{k_2+2}}\Gamma(k_2+2), \tag{106}$$

$$\begin{aligned} I_3' &= \sum_{k_1=0}^{m_1-1}\sum_{k_2=0}^{m_2-1}\frac{A_{k_1}A_{k_2}}{\eta_2^{k_2+1}}\left(\frac{d_1^{\epsilon}\sigma_r^2}{P}\right)^{k_1+1}\Gamma(1+k_2) \\ &\quad \left(\left(\frac{\eta_1 d_1^{\epsilon}\sigma_r^2}{P}\right)^{-k_1-2}\Gamma(k_1+2) - \sum_{n=0}^{k_2}\frac{1}{n!}\left(\frac{\eta_2 d_2^{\epsilon}\sigma_d^2}{\hat{P}}\right)^n \right. \\ &\quad \left. \times \left(\frac{\eta_1 d_1^{\epsilon}\sigma_r^2}{P}+\frac{\eta_2 d_2^{\epsilon}\sigma_d^2}{\hat{P}}\right)^{-k_1-n-2}\Gamma(k_1+n+2)\right), \end{aligned} \tag{107}$$

and

$$\begin{aligned} I_4' &= \sum_{k_1=0}^{m_1-1}\sum_{k_2=0}^{m_2-1}\frac{A_{k_1}A_{k_2}}{\eta_1^{k_1+1}}\left(\frac{d_2^{\epsilon}\sigma_d^2}{\hat{P}}\right)^{k_2+1}\Gamma(1+k_1) \\ &\quad \left(\left(\frac{\eta_2 d_2^{\epsilon}\sigma_d^2}{\hat{P}}\right)^{-k_2-2}\Gamma(k_2+2) - \sum_{n=0}^{k_1}\frac{1}{n!}\left(\frac{\eta_1 d_1^{\epsilon}\sigma_r^2}{P}\right)^n \right. \\ &\quad \left. \times \left(\frac{\eta_2 d_2^{\epsilon}\sigma_d^2}{\hat{P}}+\frac{\eta_2 d_1^{\epsilon}\sigma_r^2}{P}\right)^{-k_2-n-2}\Gamma(k_2+n+2)\right), \end{aligned} \tag{108}$$

for the first moment and

$$I_1'' = \left(\frac{P}{d_1^{\epsilon}\sigma_r^2}\right)^2\sum_{k_1=0}^{m_1-1}\frac{A_{k_1}}{\eta_1^{k_1+3}}\Gamma(k_1+3), \tag{109}$$

$$I_2'' = \left(\frac{\hat{P}}{d_2^{\epsilon}\sigma_d^2}\right)^2\sum_{k_2=0}^{m_2-1}\frac{A_{k_2}}{\eta_2^{k_2+3}}\Gamma(k_2+3), \tag{110}$$

$$\begin{aligned} I_3'' &= \sum_{k_1=0}^{m_1-1}\sum_{k_2=0}^{m_2-1}\frac{A_{k_1}A_{k_2}}{\eta_2^{k_2+1}}\left(\frac{d_1^{\epsilon}\sigma_r^2}{P}\right)^{k_1+1}\Gamma(1+k_2) \\ &\quad \left(\left(\frac{\eta_1 d_1^{\epsilon}\sigma_r^2}{P}\right)^{-k_1-3}\Gamma(k_1+3) - \sum_{n=0}^{k_2}\frac{1}{n!}\left(\frac{\eta_2 d_2^{\epsilon}\sigma_d^2}{\hat{P}}\right)^n \right. \\ &\quad \left. \times \left(\frac{\eta_1 d_1^{\epsilon}\sigma_r^2}{P}+\frac{\eta_2 d_2^{\epsilon}\sigma_d^2}{\hat{P}}\right)^{-k_1-n-3}\Gamma(k_1+n+3)\right), \end{aligned} \tag{111}$$

and

$$I_4'' = \sum_{k_1=0}^{m_1-1}\sum_{k_2=0}^{m_2-1}\frac{A_{k_1}A_{k_2}}{\eta_1^{k_1+1}}\left(\frac{d_2^{\epsilon}\sigma_d^2}{\hat{P}}\right)^{k_2+1}\Gamma(1+k_1)$$

$$\left(\left(\frac{\eta_2 d_2^{\epsilon}\sigma_d^2}{\hat{P}}\right)^{-k_2-3}\Gamma(k_2+3)-\sum_{n=0}^{k_1}\frac{1}{n!}\left(\frac{\eta_1 d_1^{\epsilon}\sigma_r^2}{P}\right)^{n}\times\left(\frac{\eta_2 d_2^{\epsilon}\sigma_d^2}{\hat{P}}+\frac{\eta_2 d_1^{\epsilon}\sigma_r^2}{P}\right)^{-k_2-n-3}\Gamma(k_2+n+3)\right) \tag{112}$$

for the second moment of w. Substituting I_i', $i=1,\ldots,4$ in (103) and I_i'', $i=1,\ldots,4$ in (104), and then, replacing them in (86), the $\bar{R}^{DF}$ will be achieved.

B.AF RELAY

To achieve the average ergodic rate in (87), we calculate the $\mathbb{E}[\gamma]$ and $\mathbb{E}[\gamma^2]$, where $\gamma=\gamma_2^{AF}$. So, we have

$$\mathbb{E}[\gamma]=\int_0^{\infty}\int_0^{\infty}\frac{Pz_1z_2}{x^{\epsilon}z_2\sigma_r^2+x^{\epsilon}y^{\epsilon}\sigma_d^2}\times\sum_{k_1=0}^{m_1-1}A_{k_1}z_1^{k_1}e^{-\eta_1 z_1}\sum_{k_2=0}^{m_2-1}A_{k_2}z_2^{k_2}e^{-\eta_2 z_2}dz_1dz_2 \tag{113}$$

$$=P\sum_{k_1=0}^{m_1-1}\sum_{k_2=0}^{m_2-1}A_{k_1}A_{k_2}\int_0^{\infty}\int_0^{\infty}\frac{z_1z_2}{x^{\epsilon}z_2\sigma_r^2+x^{\epsilon}y^{\epsilon}\sigma_d^2}\times z_1^{k_1}e^{-\eta_1 z_1}z_2^{k_2}e^{-\eta_2 z_2}dz_1dz_2 \tag{114}$$

The first integral on z_1 is solved using I_1 in (96) and we have

$$\mathbb{E}[\gamma]=P\sum_{k_1=0}^{m_1-1}\sum_{k_2=0}^{m_2-1}A_{k_1}A_{k_2}\eta_1^{-k_1-2}\Gamma(k_1+2)\times\int_0^{\infty}\frac{z_2}{x^{\epsilon}z_2\sigma_r^2+x^{\epsilon}y^{\epsilon}\sigma_d^2}z_2^{k_2}e^{-\eta_2 z_2}dz_2 \tag{115}$$

Now, the integral on z_2 is solved as

$$\int_0^{\infty}\frac{z_2^{k_2+1}e^{-\eta_2 z_2}}{z_2+y^{\epsilon}\sigma_d^2/\sigma_r^2}dz_2=\left(\frac{y^{\epsilon}\sigma_d^2}{\sigma_r^2}\right)^{k_2+1}\Gamma(k_2+2)\times\Gamma\left(-k_2-1,\eta_2\frac{y^{\epsilon}\sigma_d^2}{\sigma_r^2}\right) \tag{116}$$

and we have

$$\mathbb{E}[\gamma]=P\sum_{k_1=0}^{m_1-1}\sum_{k_2=0}^{m_2-1}\frac{A_{k_1}A_{k_2}}{x^{\epsilon}\sigma_r^2\eta_1^{k_1+2}}\Gamma(k_1+2)\Gamma(k_2+2)\times\left(\frac{y^{\epsilon}\sigma_d^2}{\sigma_r^2}\right)^{k_2+1}\Gamma\left(-k_2-1,\eta_2\frac{y^{\epsilon}\sigma_d^2}{\sigma_r^2}\right). \tag{117}$$

The second order of γ is achieved in the same way as

$$\mathbb{E}\left[\gamma^2\right]=\int_0^{\infty}\int_0^{\infty}\left(\frac{Pz_1z_2}{x^{\epsilon}z_2\sigma_r^2+x^{\epsilon}y^{\epsilon}\sigma_d^2}\right)^2\times\sum_{k_1=0}^{m_1-1}A_{k_1}z_1^{k_1}e^{-\eta_1 z_1}\sum_{k_2=0}^{m_2-1}A_{k_2}z_2^{k_2}e^{-\eta_2 z_2}dz_1dz_2 \tag{118}$$

$$=P^2\sum_{k_1=0}^{m_1-1}\sum_{k_2=0}^{m_2-1}\frac{A_{k_1}A_{k_2}}{\eta_1^{k_1+3}\left(x^{\epsilon}\sigma_r^2\right)^2}\Gamma(k_1+3)\times\int_0^{\infty}\frac{z_2^{k_2+2}}{\left(z_2+y^{\epsilon}\sigma_d^2/\sigma_r^2\right)^2}e^{-\eta_2 z_2}dz_2 \tag{119}$$

$$=P^2\sum_{k_1=0}^{m_1-1}\sum_{k_2=0}^{m_2-1}\frac{A_{k_1}A_{k_2}\Gamma(k_1+3)\Gamma(k_2+2)}{\eta_1^{k_1+3}\eta_2^{k_2+1}\left(x^{\epsilon}\sigma_r^2\right)^2}\times\left(e^{\frac{\eta_2 y^{\epsilon}\sigma_d^2}{\sigma_r^2}}\left(\frac{\eta_2 y^{\epsilon}\sigma_d^2}{\sigma_r^2}+k_2+2\right)E_{k_2+2}\left(\frac{\eta_2 y^{\epsilon}\sigma_d^2}{\sigma_r^2}\right)-1\right), \tag{120}$$

where $E_n(z)$ is the exponential integral function.

Substituting (115) and (120) in (87), $\bar{R}^{AF}$ is achieved. Finally, the Lemma is proved by replacing (49) for averaging on distances $x\triangleq d_1$ and $y\triangleq d_2$.

REFERENCES

[1] P. Mitra et al., "Towards 6G communications: Architecture, challenges, and future directions," in *Proc. 12th Int. Conf. Comput. Commun. Netw. Technol. (ICCCNT)*, 2021, pp. 1–7.

[2] F. Rinaldi et al., "Non-terrestrial networks in 5G & beyond: A survey," *IEEE Access*, vol. 8, pp. 165178–165200, 2020.

[3] I. Leyva-Mayorga et al., "LEO small-satellite constellations for 5G and beyond-5G communications," *IEEE Access*, vol. 8, pp. 184955–184964, 2020.

[4] O. Kodheli et al., "Satellite communications in the new space era: A survey and future challenges," *IEEE Commun. Surveys Tuts.*, vol. 23, no. 1, pp. 70–109, 1st Quart., 2021.

[5] N. Pachler, I. Del Portillo, E. F. Crawley, and B. G. Cameron, "An updated comparison of four low earth orbit satellite constellation systems to provide global broadband," in *Proc. IEEE Int. Conf. Commun. Workshops (ICC Workshops)*, 2021, pp. 1–7.

[6] "Solutions for NR to support non-terrestrial networks (NTN); Version 16.0.0," 3GPP, Sophia Antipolis, France, Rep. TR 38.821, Dec. 2019.

[7] G. Giambene, S. Kota, and P. Pillai, "Satellite-5G integration: A network perspective," *IEEE Netw.*, vol. 32, no. 5, pp. 25–31, Sep./Oct. 2018.

[8] J. G. Andrews, "Seven ways that HetNets are a cellular paradigm shift," *IEEE Commun. Mag.*, vol. 51, no. 3, pp. 136–144, Mar. 2013.

[9] C.-X. Wang et al., "On the road to 6G: Visions, requirements, key technologies, and testbeds," *IEEE Commun. Surveys Tuts.*, vol. 25, no. 2, pp. 905–974, 2nd Quart., 2023.

[10] F. Baccelli and S. Zuyev, "Stochastic geometry models of mobile communication networks," in *Frontiers in Queueing: Models and Applications in Science and Engineering*. New York, NY, USA: ACM, 1998, pp. 227–243.

[11] M. Haenggi, J. G. Andrews, F. Baccelli, O. Dousse, and M. Franceschetti, "Stochastic geometry and random graphs for the analysis and design of wireless networks," *IEEE J. Sel. Areas Commun.*, vol. 27, no. 7, pp. 1029–1046, Sep. 2009.

[12] J. G. Andrews, F. Baccelli, and R. K. Ganti, "A tractable approach to coverage and rate in cellular networks," *IEEE Trans. Commun.*, vol. 59, no. 11, pp. 3122–3134, Nov. 2011.

[13] R. Wang, M. A. Kishk, and M.-S. Alouini, "Ultra-dense LEO satellite-based communication systems: A novel modeling technique," *IEEE Commun. Mag.*, vol. 60, no. 4, pp. 25–31, Apr. 2022.

[14] H. ElSawy, E. Hossain, and M. Haenggi, "Stochastic geometry for modeling, analysis, and design of multi-tier and cognitive cellular wireless networks: A survey," *IEEE Commun. Surveys Tuts.*, vol. 15, no. 3, pp. 996–1019, 3rd Quart., 2013.

[15] D.-H. Jung, J.-G. Ryu, and J. Choi, "When satellites work as eavesdroppers," *IEEE Trans. Inf. Forensics Security*, vol. 17, pp. 2784–2799, 2022.

[16] N. Okati and T. Riihonen, "Nonhomogeneous stochastic geometry analysis of massive LEO communication constellations," *IEEE Trans. Commun.*, vol. 70, no. 3, pp. 1848–1860, Mar. 2022.

[17] N. Okati, T. Riihonen, D. Korpi, I. Angervuori, and R. Wichman, "Downlink coverage and rate analysis of low earth orbit satellite constellations using stochastic geometry," *IEEE Trans. Commun.*, vol. 68, no. 8, pp. 5120–5134, Aug. 2020.

[18] A. Talgat, M. A. Kishk, and M.-S. Alouini, "Stochastic geometry-based analysis of LEO satellite communication systems," *IEEE Commun. Lett.*, vol. 25, no. 8, pp. 2458–2462, Aug. 2021.

[19] A. Talgat, M. A. Kishk, and M.-S. Alouini, "Nearest Neighbor and contact distance distribution for binomial point process on spherical surfaces," *IEEE Commun. Lett.*, vol. 24, no. 12, pp. 2659–2663, Dec. 2020.

[20] R. Wang, M. A. Kishk, and M.-S. Alouini, "Evaluating the accuracy of stochastic geometry based models for LEO satellite networks analysis," *IEEE Commun. Lett.*, vol. 26, no. 10, pp. 2440–2444, Oct. 2022.

[21] R. Wang, A. Talgat, M. A. Kishk, and M.-S. Alouini, "Conditional contact angle distribution in LEO satellite-relayed transmission," *IEEE Commun. Lett.*, vol. 26, no. 11, pp. 2735–2739, Nov. 2022.

[22] Z. Song et al., "Cooperative satellite-aerial-terrestrial systems: A stochastic geometry model," *IEEE Trans. Wireless Commun.*, vol. 22, no. 1, pp. 220–236, Jan. 2023.

[23] A. Alsharoa and M.-S. Alouini, "Improvement of the global connectivity using integrated satellite-airborne-terrestrial networks with resource optimization," *IEEE Trans. Wireless Commun.*, vol. 19, no. 8, pp. 5088–5100, Aug. 2020.

[24] H. Kong, M. Lin, W.-P. Zhu, H. Amindavar, and M.-S. Alouini, "Multiuser scheduling for asymmetric FSO/RF links in satellite-UAV-terrestrial networks," *IEEE Wireless Commun. Lett.*, vol. 9, no. 8, pp. 1235–1239, Aug. 2020.

[25] G. Pan, J. Ye, Y. Zhang, and M.-S. Alouini, "Performance analysis and optimization of cooperative satellite-aerial-terrestrial systems," *IEEE Trans. Wireless Commun.*, vol. 19, no. 10, pp. 6693–6707, Oct. 2020.

[26] Y. Ma, T. Lv, T. Li, G. Pan, Y. Chen, and M.-S. Alouini, "Effect of strong time-varying transmission distance on LEO satellite-terrestrial deliveries," *IEEE Trans. Veh. Technol.*, vol. 71, no. 9, pp. 9781–9793, Sep. 2022.

[27] R. Wang, M. A. Kishk, and M.-S. Alouini, "Reliability analysis of multi-hop routing in multi-tier LEO satellite networks," *IEEE Trans. Wireless Commun.*, vol. 23, no. 3, pp. 1959–1973, Mar. 2024.

[28] A. Tovchigrechko and I. A. Vakser, "How common is the funnel-like energy landscape in protein-protein interactions?" *Protein Sci.*, vol. 10, no. 8, pp. 1572–1583, 2001.

[29] C. Loo, "A statistical model for a land mobile satellite link," *IEEE Trans. Veh. Technol.*, vol. 34, no. 3, pp. 122–127, Aug. 1985.

[30] X. Zhang et al., "Outage performance of NOMA-based cognitive hybrid satellite-terrestrial overlay networks by amplify-and-forward protocols," *IEEE Access*, vol. 7, pp. 85372–85381, 2019.

[31] N. I. Miridakis, D. D. Vergados, and A. Michalas, "Dual-hop communication over a satellite relay and shadowed Rician channels," *IEEE Trans. Veh. Technol.*, vol. 64, no. 9, pp. 4031–4040, Sep. 2015.

[32] Y. Zhang, S. Feng, and W. Tang, "Performance analysis of hybrid cellular and bidirectional device-to-device cooperative NOMA communication systems," *IEEE Trans. Veh. Technol.*, vol. 70, no. 10, pp. 10420–10435, Oct. 2021.

[33] I. S. Gradshtein, A. Jeffrey, I. M. Ryzhik, and D. Zwillinger, *Table of Integrals, Series, and Products*. Amsterdam, The Netherlands: Elsevier, 2007.